Received: 6 June 2020 | Revised: 10 September 2020 | Accepted: 28 September 2020

DOI: 10.1002/btpr.3090

RESEARCH ARTICLE

BIOTECHNOLOGY PROGRESS

Induced pluripotent stem cells can utilize lactate as a metabolic substrate to support proliferation

Daniel C. Odenwelder[1] | Xiaoming Lu[1,2] | Sarah W. Harcum[1]

[1]Department of Bioengineering, Clemson University, Clemson, South Carolina

[2]Department of Biomolecular and Chemical Engineering, Clemson University, Clemson, South Carolina

Correspondence
Sarah W. Harcum, Department of Bioengineering, Clemson University, Clemson, SC 29634-0905.
Email: harcum@clemson.edu

Present address
Daniel C. Odenwelder, Gene Therapy Upstream Process Development, Biogen, Cambridge, Massachusetts

Funding information
Advanced Mammalian Biomanufacturing Innovation Center (AMBIC), Grant/Award Number: AMBIC 2016-01; National Science Foundataion, Grant/Award Numbers: CBET-1218345, IIP-1624641, OIA-1736123

Abstract

Human-induced pluripotent stem cells (iPSCs) hold the promise to improve cell-based therapies. Yet, to meet rising demands and become clinically impactful, sufficient high-quality iPSCs in quantity must be generated, a task that exceeds current capabilities. In this study, K3 iPSCs cultures were examined using parallel-labeling metabolic flux analysis (^{13}C-MFA) to quantify intracellular fluxes at relevant bioprocessing stages: glucose concentrations representative of initial media concentrations and high lactate concentrations representative of fed-batch culture conditions, prior to and after bolus glucose feeds. The glucose and lactate concentrations are also representative of concentrations that might be encountered at different locations within 3D cell aggregates. Furthermore, a novel method was developed to allow the isotopic tracer [U-$^{13}C_3$] lactate to be used in the ^{13}C-MFA model. The results indicated that high extracellular lactate concentrations decreased glucose consumption and lactate production, while glucose concentrations alone did not affect rates of aerobic glycolysis. Moreover, for the high lactate cultures, lactate was used as a metabolic substrate to support oxidative mitochondrial metabolism. These results demonstrate that iPSCs have metabolic flexibility and possess the capacity to metabolize lactate to support exponential growth, and that high lactate concentrations alone do not adversely impact iPSC proliferation.

KEYWORDS

bioprocessing, induced pluripotent stem cells, scale-up, Warburg effect

1 | INTRODUCTION

Human embryonic stem cells (hESCs) and induced pluripotent stem cells (iPSCs) are considered to be dependent on aerobic glycolysis and lactate fermentation for energy production.[1-3] In addition, during somatic cell nuclear reprogramming, iPSCs have been shown to shift from oxidative phosphorylation to aerobic glycolysis upon the acquisition of pluripotency.[4-7] Stimulation of glycolysis has also been observed to promote maintenance of stemness for pluripotent stem cells (PSCs) and augmented somatic reprogramming to iPSCs, while inhibition of specific glycolytic reactions in turn inhibited reprogramming.[6,8,9] On the other hand, inhibition of glycolysis was shown to promote spontaneous differentiation, suggesting that metabolism plays a functional role in regulating cell self-renewal and differentiation.[1,3,10] This reliance on glycolysis over oxidative phosphorylation in well-oxygenated systems is a metabolic phenotype called the Warburg effect, and is also a characteristic of cancer cell metabolism.[4,11-13] However, unlike cancer cells, which can catabolize lactate for energy, PSCs are hypothesized to be highly sensitive to lactate accumulation.[14-21] Specifically, hESCs exhibited decreased pluripotency after serial passage in 11 mM lactate-containing media.[19] Moreover, elevated lactate and glucose-depleted media has previously been shown to preferentially induce cardiomyocyte differentiation for iPSCs.[22] Thus, current PSC culture techniques require frequent media exchange to alleviate lactate stresses.[23,24] Since lactate accumulation appears to be an unavoidable byproduct of iPSC metabolism,

deciphering the role of accumulated extracellular lactate on intracellular iPSC metabolism and understanding the regulatory role of glucose concentration to modulate lactate production are crucial.

Metabolic flux analysis (MFA) is a powerful computational technique used to determine intracellular metabolic pathway fluxes.[25,26] In MFA, intracellular fluxes are determined by coupling extracellular metabolite uptake and secretion rates with a discrete stoichiometric metabolic network model.[27] This technique is frequently used to compare metabolism of different cell lines and cell culture conditions to assess the activity of individual pathways under each condition.[28] There are two primary MFA approaches: stoichiometric MFA, which uses mass balance to determine intracellular metabolic fluxes from extracellular consumption and production fluxes, and ^{13}C-MFA, in which stable isotope tracers are used to provide intracellular measurements to resolve fluxes through more complex metabolic pathways.[27,29,30]

The aims of this study were to determine the metabolic contribution of glucose and extracellular lactate to iPSC metabolism, and in particular, to determine (a) whether lactate can serve as a metabolic substrate in support of iPSC proliferation and (b) if glucose concentration can modulate lactate production. K3 iPSCs were grown in both low and normal glucose-containing media and with and without extracellular lactate additions. The low glucose and high lactate concentrations were selected such that exponential growth rates for the cultures were maintained across the four conditions, as would be desired in large-scale cultivation. The pluripotency and differentiation capacity of the iPSCs were assessed from each culture condition to determine if glucose or lactate concentration impacted these phenotypes. Parallel labeling experiments were conducted with [1,2-$^{13}C_2$] glucose, [U-$^{13}C_5$] L-glutamine, and [U-$^{13}C_3$] sodium L-lactate, while the control and low glucose cultures were labeled with [1,2-$^{13}C_2$] glucose and [U-$^{13}C_5$] L-glutamine only, since lactate was not added to these cultures. Metabolic flux maps were generated for each condition to compare the resulting flux distributions from culturing iPSCs in low glucose and high lactate culture media. To our knowledge, this is the first ^{13}C-MFA study to investigate the metabolic flexibility of iPSCs with respect to lactate catabolism.

2 | MATERIALS AND METHODS

2.1 | Cell culture

K3 iPSCs were donated by Dr. Stephen A. Duncan at the Medical University of South Carolina. The K3 iPSCs were generated by transient transfection of human foreskin fibroblast cells.[31] K3 iPSCs were grown on non-tissue culture treated 6-well plates and 60 mm cell culture dishes (Corning Inc., Corning, NY) coated with 10 μg/mL StemAdhere™ (Primorigen, Cat. no. S2071-500UG) per manufacturer instructions[32] at 37°C and in a humidified 5% CO_2 incubator in Essential 8 Flex™ (E8 Flex) media (Thermo Fisher Scientific, Waltham, MA). The working volume of media was 3 mL per well in the 6-well plates and 6.5 mL for the 60 mm cell culture dishes. Cells were maintained by passaging every 3 days at 1:6 and 1:12 depending on confluency. Accutase (Sigma-Aldrich, St. Louis, MO) was used to passage cells, 2 min at 37°C and washed with phosphate buffered saline (PBS) without calcium or magnesium (Corning Inc., Corning, NY). Detached cells were centrifuged at 500*g* for 5 min and resuspended in fresh E8 Flex supplemented with 10 μM Y-27632—rho-associated, coiled-coil containing protein kinase inhibitor (ROCKi) (Stem Cell Technologies, Vancouver, Canada). After 24 hr, the medium was replaced with E8 Flex without ROCKi. For the cell growth and parallel labeling experiments, E8 Flex medium without glucose and glutamine was used. The initial media concentrations are listed in Table 1 for the four culture conditions. The control growth media is the standard E8 Flex media concentrations. D-glucose (Fisher Scientific, Hampton, NH), L-glutamine (Corning Inc., Corning, NY), sodium L-lactate (Sigma-Aldrich, St. Louis, MO), and sodium chloride (Fisher Scientific, Hampton, NH) were added to unlabeled experiments at concentrations as indicated in Table 1. [1,2-$^{13}C_2$] D-glucose (99% enrichment), [U-$^{13}C_5$] L-glutamine (99% enrichment), and [U-$^{13}C_3$] sodium L-lactate (98% enrichment) isotope tracers were used for the parallel labeling experiments (Cambridge Isotope Laboratories, Tewksbury, MA), and added to the labeled experiments at concentrations matching E8 Flex or as indicated.

2.2 | Cell growth and parallel labeling experiments

For the growth and isotope labeling studies, K3 iPSCs were seeded at 1.0 x 10^4 cells/cm^2 in E8 Flex with 10 μM ROCKi to allow for cell attachment and reduce apoptosis associated with single cell detachment and passaging.[33] After 24 hr, a media exchange was performed, and the growth media was introduced to the parallel 6-well plates and 60 mm cell culture dishes (indicated as Time 0 hr in Figure 1). For clarity, a schematic of the full experimental setup is shown in Figure 1. In all, six 6-well plates and eighteen 60-mm cell culture dishes were used per high lactate and low glucose + high lactate conditions, and six 6-well plates and twelve 60-mm dishes were used per control and low glucose conditions. E8 Flex was provided without glucose and glutamine, such that glucose could be supplemented at different concentrations and labeled glucose and glutamine could be used for the ^{13}C-MFA studies. The control growth media contained 18.3 mM glucose and 2.75 mM L-glutamine to reflect the standard E8 Flex media concentrations. Table 1 lists the media concentrations used for each condition, including the glucose, lactate, and glutamine concentrations and the supplemented sodium chloride concentration. An initial screening study was performed to determine the minimum glucose concentration that did not result in glucose depletion prior to 48 hr. Non-zero glucose concentrations were important to ensure that glucose was not the limited during exponential growth, which then allowed for the assumption of pseudo steady state. Recently, media acidosis was shown to negatively impact hPSC, with low pH resulting in decreased glucose consumption, cell cycle arrest, and cell death.[34] Therefore, sodium L-lactate was used as the lactate source to avoid pH shifts due to the lactate addition and to decouple the effects

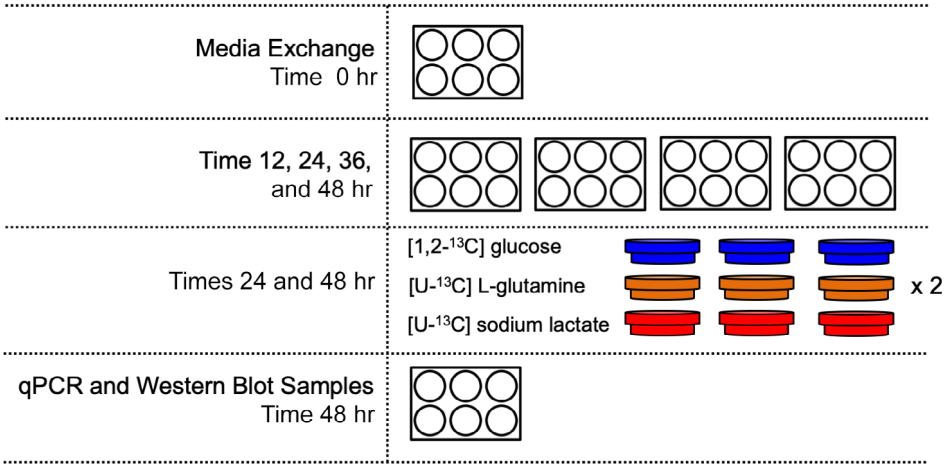

FIGURE 1 Parallel isotope labeling and culture replicate setup for each condition. All 6-well plates and 60 mm cell culture dishes were seeded in parallel 24 hr prior to the media exchange (Time 0 hr). The times shown indicate when the plates or dishes were harvested for analysis relative to the isotope media exchange. The 60 mm cell culture dishes contained isotopically labeled media, which were used to obtain for intracellular isotope MID values. The 6-well plates were used to measure cell number, glucose, lactate, pyruvate, and amino acid concentrations, individually by well. Isotopic labeling is graphically shown by shading (clear—no isotope, blue—[1,2-$^{13}C_2$] glucose, orange—[U-$^{13}C_5$] L-glutamine, and red—[U-$^{13}C_3$] sodium lactate)

TABLE 1 Media formulations for iPSC cultures examined in ^{13}C-MFA studies

	^{13}C-MFA growth media cultures			
	Concentrations (mM)			
Component	Control	High lactate	Low glucose	Low glucose + High lactate
Glucose	18.3	18.3	5.6	5.6
L-glutamine	2.75	2.75	2.75	2.75
Sodium L-lactate	-	20.0	-	20.0
Added sodium chloride	+ 20.0	-	+ 20.0	-

Note: The initial glucose, glutamine, sodium L-lactate, and added sodium chloride concentrations are listed for the time corresponding to the isotope labeling (media exchange) addition. Sodium chloride was added to balance osmolarity in cultures without sodium lactate.

of pH and lactate on K3 iPSC phenotype. An equal molar concentration of sodium chloride was added to the non-lactate cultures to balance osmolarity, as described in the materials and method section. A screening study was also performed to determine the maximum sodium lactate concentration that could be used without growth rates inhibit within the normal lactate concentrations reported to occur in cell culture.[19-21] Another objective of the growth screening with glucose and lactate concentrations was to ensure equivalent growth rates between the cultures under all four conditions; this allowed for any observed metabolic flux differences to be attributed to the media differences and not differences in biomass accumulation.

Inoculum was used across multiple conditions, such that no condition had only a single inoculum. To limit media carryover, cells were washed with PBS for 5 min at room temperature prior to adding the growth media. Cell numbers and extracellular metabolite concentrations were measured at: 0, 12, 24, 36, and 48 hr after the media exchange. Cell numbers, glucose, lactate, pyruvate, ammonia, and amino acid extracellular measurements were obtained from the 6-well plates. The intracellular mass isotope distributions (MIDs) were obtained from 60-mm cell culture dishes at 24 and 48 hr. The control and low glucose cultures had parallel labeling with [1,2-$^{13}C_2$] glucose and [U-$^{13}C_5$] L-glutamine, whereas the high lactate and low glucose + high lactate cultures had parallel labeling with [1,2-$^{13}C_2$] glucose, [U-$^{13}C_5$] L-glutamine, and [U-$^{13}C_3$] sodium L-lactate. Cell numbers were obtained using the Vi-Cell XR cell viability analyzer (Beckman Coulter, Brea, CA). Extracellular glucose, lactate, pyruvate, glutamine, glutamate, and ammonia concentrations were measured using a Cedex Bio (Roche Diagnostics, Mannheim, Germany).

2.3 | Derivatization and GC-FID analysis of extracellular amino acids

Extracellular amino acid concentrations were measured from the cell culture supernatant by derivatization using the EZ: faast™ amino acid analysis kit (Phenomenex, Torrance, CA). Standard were prepared for amino acids—alanine, asparagine, aspartic acid, glycine, histidine, isoleucine, leucine, lysine, phenylalanine, proline, serine, threonine,

tryptophan, tyrosine, and valine—to a final concentration of 10 mM in water and pH adjusted to below pH 7.0. Standard curves were generated for each amino acid. Samples (150 μL) and 50 μL of an internal standard (200 μM norvaline) were derivatized as per manufacturer instructions.[35] Derivatized samples were analyzed using a gas chromatography-flame ionization detector (GC-FID) instrument (Agilent Technologies, 7890A GC system) equipped with an autosampler (Agilent Technologies, 7683B Series Injector). A Zebron ZB-AAA 10 m x 0.25 mm capillary GC column with an initial column temperature 60°C which increased by 32°C/min to a final temperature of 320°C. The FID detector temperature was 320°C and 2 μL of sample was injected at an injection temperature of 250°C and a split ratio of 1:15 using a 10 μL syringe (Agilent Technologies, Part # 5181–1,267). Helium was used as the carrier gas at 1.5 mL/min constant flow.

2.4 | Extraction of intracellular metabolites

At 24 and 48 hr, the culture media was removed from the 60 mm cell culture dishes to remove debris and detached cells. The attached cells were washed with 3 mL of cold PBS (4°C) for 5 min. Then, 1 mL of cold methanol (−20°C, LC/MS grade) was added and incubated on ice for 5 min. Adherent cells were removed from the dishes using a cell scraper. The collected cell suspensions from the dishes were then transferred to 15 mL glass centrifuge tubes (with Teflon-sealed caps) which contained 1 mL s. Next, 1 mL of water was added to each tube, and samples were vortexed vigorously for 1 min. All sample tubes were stored overnight at 4°C. After overnight storage, all tubes were centrifuged at 4000*g* at 4°C for 20 min to fully separate the aqueous and organic phases. The upper aqueous phase (methanol and water) contained the polar intracellular metabolites and the lower organic phase (chloroform) contained the non-polar metabolites (fatty acids). Each phase was transferred to separate GC vials for further analysis. The metabolism quenching and separation procedure was adapted from Ahn and Antoniewicz (2013).

2.5 | Derivatization and GC–MS analysis of intracellular metabolites

The aqueous phases were evaporated to dryness using a CentriVap (Labconco, Kansas, MO). Dried samples were then dissolved in 10 μL of methoxyamine hydrochloride (Sigma-Aldrich, St. Louis, MO) and incubated with shaking at 30°C and 1,000 rpm for 90 min in an Echo-Therm™ SC20 Orbital Mixing Dry Bath (Torrey Pines Scientific, Inc., Carlsbad, CA). Next, 90 μL of N-methyl-N-(tert-butyldimethylsilyl)-trifluoroacetamide (MTBSTFA) (Sigma-Aldrich, St. Louis, MO) was added to samples to initiate trimethylsilylation. The trimethylsilylation reaction was incubated with shaking at 37°C and 1,000 rpm for 60 min. MTBSTFA containing C8–C30 fatty acid methyl esters (FAMEs) was used as a set of internal standards to determine retention times. Derivatized samples were submitted to a Leco Pegasus IV time-of-flight MS (Leco Corporation) with electron ionization mode at −70 eV. A Rtx-5Sil MS column (30 m x 0.25 mm, 0.25 μm) was used. The initial temperature was 50°C, held for 1 min, then increased to 330°C at 20°C/min, then held for 5 min. The flow rate was set to 1.0 mL/min and 0.5 μL of sample was injected. Mass spectrometry detector voltage was 1,525 V. Data was acquired at 17 spectra/s with scan range from 85 to 600 Da. Ion source temperature was 250°C and transfer line temperature was 280°C. Standard mixture and blank samples were injected at the beginning of the analysis and every 10 samples throughout the analysis for quality control. The GC–MS analysis was conducted at the West Coast Metabolomics Center at the University of California, Davis, CA.

2.6 | Determination of biomass specific consumption and production rates

Extracellular glucose, lactate, pyruvate, and amino acid fluxes were calculated using measured concentrations and growth profiles via the Extracellular Time-Course Analysis (ETA) software available for Matlab.[36] The ETA software uses a Gaussian error propagation approach to calculate fluxes and *SE*s from averaged time series data. This software was also used to assess the goodness-of-fit of measured experimental data to a linear regression model. The glutamine decomposition rate constant (k) was determined for E8-Flex media to be 0.00178 hr^{-1} using media without cells held at 37°C for 72 hr.

2.7 | Dry cell weight measurements

K3 iPSCs were cultured in E8 Flex media were harvested from six 100 mm non tissue culture treated dishes at ∼90% confluence. Pairs of plates were combined to give triplicate dry cell weights. Cells were washed with 5 mL PBS for 5 min, then detached using Accutase for 2 min at 37°C. Cells were pelleted by centrifuging at 5000*g* for 5 min. The supernatant was removed, and cells were resuspended in 10 mL of water by briefly vortexing. Next, cells were centrifuged again at 5000*g* for 5 min. Finally, the water was removed, and the cell pellets were resuspended in 1–2 mL of water, vortexed, and transferred to aluminum drying pans. Cell pellets were dried in ambient air at 95°C for 2 days.

2.8 | Metabolic network model

A generalized mammalian cell model focused on central carbon metabolism was used to model iPSC metabolism, adapted from several previously published metabolic frameworks.[37-39] The iPSC model contained the major reactions for glucose consumption, the TCA cycle, amino acid metabolism, lactate metabolism, and fatty acid metabolism. Early glycolysis and the pentose phosphate pathway (PPP) reactions were not included in the iPSC model since the intracellular MIDs for these metabolites were poorly resolved experimentally. This approach to simplify glycolysis and PPP is similar to the approach used in Jiang et al. 2016. The carbon flux to the biomass

was divided into two compartments—termed the biomass pool and the "lipid biomass" pool.[37,39-41] The biomass fraction contains nucleotides, proteins, and carbohydrates, and lipid biomass fractions contains acetyl-CoA. The relative weight fraction of the biomass and lipid biomass pools are 0.9 and 0.1, respectively, based on cell mass composition of hybridoma cells and the experimentally measured dry cell weight for K3 iPSCs and the experimentally determined iPSC growth rates.[40] A full description of the metabolic model with assumptions can be found in Appendix C. The full list metabolic reactions including the atom carbon transitions is included in Appendix D.

2.9 | Metabolic flux analysis

^{13}C-MFA was conducted using the Isotopomer Network Compartmental Analysis (INCA) software package.[42] INCA utilizes the elementary metabolite unit framework to perform MID simulations, and is capable of performing both isotopic steady-state and isotopic non-stationary MFA.[43,44] For this work, isotopic steady-state MFA was conducted to estimate intracellular metabolic fluxes, where extracellular uptake and secretion fluxes, coupled with intracellular MIDs from the 24 hr samples. INCA software was used for the ^{13}C-MFA for the parallel labeling experiments, a process that has been shown to improve flux resolution throughout intracellular metabolism.[45,46] Flux estimations were performed for 100 restarts from initial random guesses. This increased the likeliness that a global solution would be obtained.[47]

2.10 | Extended expansion of K3 iPSCs

K3 iPSCs were cultured for five passages in each of the four culture media to assess the effects of glucose and lactate on iPSC proliferation and pluripotency. The cell culture and passage procedures were as described in section 2.2. After five passages, cell pellets were obtained and stored at −80°C for gene and protein expression analysis via real-time quantitative reverse transcriptase polymerase chain reaction (qRT-PCR) and western blot, respectively.

2.11 | RNA extraction and qRT-PCR

Total mRNA was isolated from K3 iPSCs at 48 hr using a RNeasy® Plus Mini Kit (Qiagen Inc., Valencia, CA) and QIAshredder (Qiagen Inc., Valencia, CA) according to the manufacturer's instructions. Isolated RNA sample quality assessment and quantification was performed using a NanoDrop™ 8,000 Spectrophotometer (Thermo Fisher Scientific, Waltham, MA). Real-time qRT-PCR was performed using the iTaq™ Universal SYBR® Green One-Step Kit (Bio-Rad Laboratories, Inc., Hercules, CA). qRT-PCR was carried out using the iQ™5 cycler (Bio-Rad Laboratories, Inc., Hercules, CA) with the following program: reverse transcription for 10 min at 50°C; polymerase activation and DNA denaturation for 1 min at 95°C; 40 cycles at 95°C for 10 s, 58.6°C for 15 s, and 72°C for 15 s. Relative expression was determined using the $\Delta\Delta C_T$ method with Gapdh used as an internal standard.[48] Primer sequences are listed in Table 2. Gapdh, Oct4, Sox2, and Nanog primers were purchased from Integrated DNA Technologies (IDT, Coralville, IA).

2.12 | Western blots

Whole cell and embryoid body lysates were prepared using 1X Cell Lysis Buffer (Cell Signaling Technology, Danvers, MA) containing 1X Halt™ Protease and Phosphatase Inhibitor C (Thermo Fisher Scientific, Waltham, MA). The cell lysate protein concentration was quantified using the Pierce™ BCA Protein Assay Kit (Thermo Fisher Scientific, Waltham, MA). Samples were loaded at a concentration of 5 μg of total protein per well. Protein separation was performed on 4–15% Mini-PROTEAN® TGX™ Precast Gels (Bio-Rad Laboratories, Inc., Hercules, CA). Immun-Blot® PVDF (polyvinylidene difluoride) membranes were used (Bio-Rad Laboratories, Inc., Hercules, CA). Non-specific protein binding to the PVDF membrane was blocked using 5% non-fat dried milk in Tris buffered saline (TBS) at room temperature on an orbital shaker for 1 hr. Overnight primary antibody incubation was performed at 4°C. Each primary antibody was diluted at 1:1000 in TBST—β-actin (Fisher Scientific, Hampton, NH) and Oct4 (Novus Biologicals, Centennial, CO). The secondary antibody incubations were conducted for 1 hr at room temperature at a 1:1000 dilution in TBST using a goat anti-rabbit IgG HRP-linked antibody for β-actin and a goat anti-mouse IgG HRP-linked antibody for Oct4 (Bio-Rad Laboratories, Inc., Hercules, CA). Protein detection was obtained using the Vector® VIP peroxidase substrate kit (Vector Laboratories, Burlingame, CA) and quantified by densitometry using Image Studio Lite (Licor).

2.13 | Statistical analysis

Statistical analysis was performed using JMP Pro 14 software (SAS Institute, Cary, NC). The generalized linear model (GLM) procedure

TABLE 2 PCR primer sequences for analysis of K3 iPSCs

Gene	Forward primer sequence (5′→3′)	Reverse primer sequence (5′→3′)
Gapdh	CTGGGCTACACTGAGCACC	AAGTGGTCGTTGAGGGCAATG
Oct4	CTTGAATCCCGAATGGAAAGGG	CCTTCCCAAATAGAACCCCCA
Nanog	TTTGTGGGCCTGAAGAAAACT	AGGGCTGTCCTGAATAAGCAG
Sox2	GCCGAGTGGAAACTTTTGTCG	GGCAGCGTGTACTTATCCTTCT

Note: Primer sequences used for qPCR analysis of pluripotency and germ-layer differentiation for K3 iPSCs.

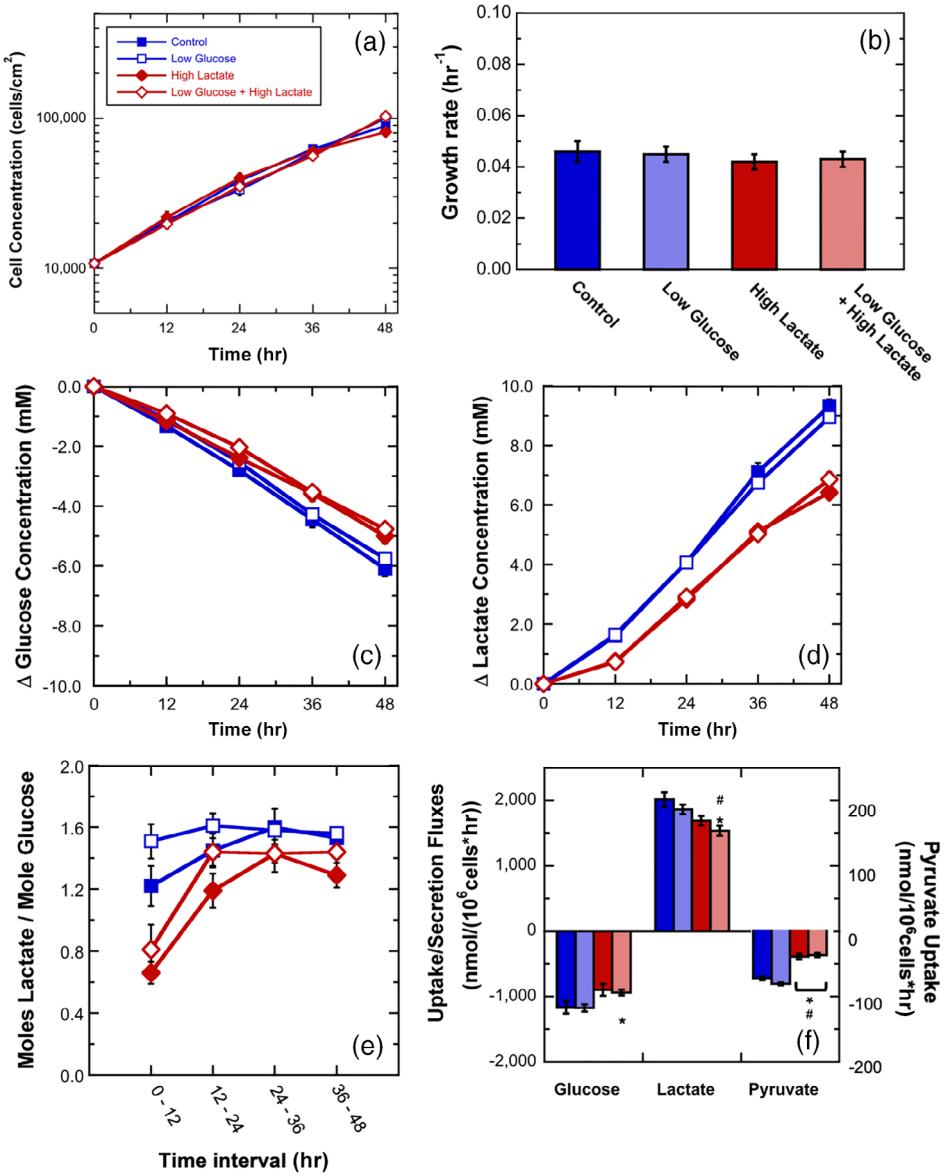

FIGURE 2 Growth characteristics of K3 iPSC cultures in low and high glucose and lactate containing media. (a) Growth profiles. The isotope media exchange occurred at 0 hr and samples for MID analysis were taken at 24 and 48 hr. (b) Growth rates for the times 0 to 36 hr. (c) Net glucose consumption. (d) Net lactate production. (e) Glycolytic efficiencies. (f) Calculated glucose consumption, pyruvate consumption, and lactate production fluxes from 12 to 36 hr. Line graphs: Control media—blue square filled; Low Glucose media—blue square open; High Lactate media—red diamond filled; and Low Glucose + High Lactate—red diamond open. Bar graph: Control (blue), Low Glucose (light blue), High Lactate (red), and Low Glucose + High Lactate (light red). The asterisk (*) indicates the calculated flux was significantly different from the control condition ($p \leq .05$). The pound (#) indicates the calculated flux was significantly different from the low glucose condition ($p \leq .05$). Error bars represent *SE*s

($p \leq 0.05$) and least squares method with Tukey HSD (honest significant difference) were used to determine if cell number, extracellular metabolite concentrations, gene expression, and protein expression were significantly different between conditions ($p \leq 0.05$). An ANCOVA (analysis of covariance) was also used to determine if metabolite consumption and production profile slopes were significantly different between conditions ($p \leq 0.05$). Student's two-tailed t-tests were used to determine if the extracellular fluxes and intracellular MIDs were significantly different between conditions ($p \leq 0.05$). For ^{13}C-MFA model convergence in INCA, an acceptable simulation fit was determined to occur when a global solution was reached that satisfied the accepted weighted sum of squared residuals criteria between the input measurements and simulated measurement outputs. A chi-squared statistical test and sensitivity analysis were performed to determine goodness-of-fit and 95% confidence intervals for each predicted flux, respectively.[49,50]

3 | RESULTS AND DISCUSSION

3.1 | Cell growth

To determine the effects of low glucose and high extracellular lactate concentrations on iPSC metabolism, K3 iPSCs were grown in media containing either typical glucose concentrations (18.3 mM) or low glucose concentrations (5.6 mM). Also, cultures were either exposed to high extracellular lactate (20 mM) or not exposed to high extracellular lactate. Cell counts were taken every 12 hr to characterize cell growth; growth profiles from each condition are shown in Figure 2a. The media exchange described in the materials and methods section The media exchange is indicated by time 0 hr in Figure 2a. For the parallel labeling experiments, ^{13}C isotopes replaced the unlabeled glucose, glutamine, or lactate in the culture media at the same concentration. Dry cell weight measurements were used to determine the biomass specific flux associated with

cell growth. The dry cell weight for K3 iPSC was 263 ± 15 pg/cell (mean ± *SEM*); this measured dry cell weight is similar to those previously reported for two hESC lines cultured in Essential 8 medium—HUES 9 hESC (250 pg/cell) and H9 hESC (200 pg/cell).[51] Exponential growth was observed for all culture conditions for 48 hr. Growth rates were calculated from 0 to 36 hr and were similar between the four conditions ($p > 0.05$). The similar growth rates shown in Figure 2b confirm that the glucose and lactate concentrations did not significantly affect the K3 iPSCs growth rates. Previously, murine PSCs have been shown to be capable of proliferate in up to 40 mM lactate, while human PSCs growth rates were noted to decrease in 11 mM lactate containing media.[19,20,52,53] Yet, for the K3 iPSCs, the low glucose and high lactate culture concentrations did not inhibit growth.

3.2 | Glucose, lactate, and amino acid metabolism

PSCs are dependent on glucose catabolism and lactate production to support cell growth.[1-3] To characterize glucose consumption and lactate production for K3 iPSCs, extracellular glucose and lactate concentrations were measured at 0, 12, 24, 36, and 48 hr after the media exchange. Figure 2c,d shows the change in glucose and lactate concentrations with time for each culture. The data were normalized to show change in concentration, since the initial media concentrations of glucose and lactate were greatly different. K3 iPSCs exhibited equal growth rates for each of the four conditions (Figure 2b); however, the high extracellular lactate resulted in decreased glucose consumption and reduced lactate accumulation for both high lactate conditions ($p \leq 0.05$). Low glucose alone did not significantly impact the glucose consumption or lactate production rates ($p > 0.05$). The average glucose and lactate concentrations for all the 0, 12, 24, 36, and 48 hr samples are listed with *SE* in Appendix A, Tables A1–A4. Additionally, Figure 2f shows the pyruvate uptake flux for 12 to 36 hr. Both high lactate cultures had decreased pyruvate consumption fluxes ($p \leq 0.05$), whereas the glucose concentration did not have a significant effect on the pyruvate flux ($p > 0.05$). The pyruvate concentration in E8 Flex basal media is only 0.4 mM, and it was observed to be depleted between 36 and 48 hr.

Initially, each high lactate culture exhibited a decreased glycolytic efficiency for the first 12 hr of culture (Figure 2e). Then, from 12 to 48 hr, the glycolytic efficiencies were similar across the four conditions. Glycolytic efficiency is defined as the moles of lactate produced per mole of glucose consumed, with the theoretical maximum glycolytic efficiency being 2.0 mol of lactate produced per mole of glucose consumed. The initial difference in glycolytic efficiencies between the high lactate cultures and the control and low glucose cultures potentially illustrates an initial shift in glucose to lactate metabolism or more likely a lactate shock. This also suggests that iPSCs in the high lactate cultures may not have been at a metabolic steady-state through the first 12 hr of growth; therefore, concentration changes during the first 12 hr of growth were excluded from flux calculations. Specifically, the low initial glycolytic efficiencies observed immediately following the media exchange (between 0 and 12 hr) for each high lactate culture may be the result of a high initial lactate exchange across the cell membrane (Figure 2e), since lactate is transported across the cell membrane through facilitated diffusion by proton-linked monocarboxylate transporters (MCTs).[54,55] Similarly, pyruvate transport across the plasma membrane is also facilitated by MCTs.[55] Therefore, the decreased pyruvate consumption in both high lactate culture conditions could be a result of more favorable lactate transport kinetics.[56] Also, since the glycolytic efficiency observed was always less than 2.0, glucose was not stoichiometrically converted to lactate, as has previously been reported for hESC.[6,57] Nevertheless, the similar glycolytic efficiencies between 12 and 48 hr suggest that the same proportion of glucose was catabolized to lactate in each condition, and only the net glucose consumed decreased for the cells grown in high lactate.

Proliferating cells require significant protein and nucleotide synthesis to maintain rapid growth.[40] As a result, amino acid catabolism plays a critical anaplerotic role in PSC metabolism.[58] Extracellular amino acid concentrations were measured at 0, 12, 24, 36, and 48 hr after the media exchange in order to assess amino acid fluxes. First, statistical analysis was performed to determine if amino acid concentrations were significantly different over time and between the conditions. Asparagine, glycine, lysine, proline, tryptophan, and tyrosine concentrations did not significantly change with respect to time ($p > 0.05$). Extracellular fluxes were not calculated for these amino acids that did not have significant time dependences. All other amino acid concentrations varied significantly with time; and, fluxes were determined for these amino acids. Only the serine concentrations did not vary between the culture conditions ($p > 0.05$); however, alanine, aspartate, glutamine, glutamate, histidine, isoleucine, leucine, lysine, methionine, phenylalanine, threonine, and valine concentrations varied between culture conditions ($p \leq 0.05$). Table 3 lists the calculated amino acid fluxes with *SE* for the amino acids with time dependences. The average amino acid concentrations for all the 0, 12, 24, 36, and 48 hr samples are listed with *SE* in Appendix A, Tables A1–A4. Amino acid concentration time profiles are included in Appendix B.

High extracellular lactate also caused reduced glutamine consumption, glutamate production, and ammonia accumulation for both high lactate conditions ($p \leq 0.05$); however, the moles of ammonia produced per moles of glutamine consumed remained relatively constant for each of the four culture conditions. Figure 3 shows the change in glutamine, glutamate, and ammonia concentrations with time for each culture. Lactate has previously been suggested to inhibit ammonia secretion in a number of mammalian cell lines.[59,60] Two potential mechanisms for this are (a) the metabolic conversion of lactate to pyruvate promotes alanine production and reduces ammonia accumulation, or (b) lactate inhibits glutaminase activity—the enzyme responsible for converting glutamine to glutamate.[59,60] While alanine production did not increase due to high lactate, glutamine consumption decreased for both high lactate cultures. These results suggest that high extracellular lactate inhibits glutamine consumption and ammonia production.

TABLE 3 Experimentally determined biomass specific uptake and production rates for extracellular metabolite (nmol/10^6 cells·hr)

	Fluxes (nmol/10^6 cells·hr)							
	Control		Low glucose		High lactate		Low glucose + High lactate	
Metabolite	Flux	*SE*	Flux	*SE*	Flux	*SE*	Flux	*SE*
Glucose	−1,164	97.0	−1,176	55.1	−897	90.8	−937	43.5
Lactate	2013	113	1861	72.4	1,692	73.4	1,537	76.2
Pyruvate	−67.6	2.6	−75.3	2.0	−38.6	3.6	−36.5	2.6
Ammonia	135	5.1	125	5.7	105	8.4	107	5.5
Alanine	33.3	2.1	32.2	1.5	28.8	3.5	27.7	3.1
Aspartate	−0.4	0.5	−3.5	0.2	0.3	0.4	−1.8	1.0
Glutamate	36.1	1.7	32.3	1.2	28.3	1.4	29.4	1.6
Glutamine	−141	16.9	−155	9.0	−107	9.6	−119	9.5
Histidine	1.1	3.2	−14.7	1.9	−0.6	2.2	0.0	1.4
Isoleucine	−56.7	10.0	−39.3	5.6	−24.7	6.9	−45.4	8.4
Leucine	−41.8	7.0	−31.3	2.6	−9.8	4.2	−20.9	4.8
Methionine	−7.4	1.6	−4.4	1.1	−0.4	1.5	−0.5	1.9
Phenylalanine	−7.6	4.3	−7.7	2.2	7.8	1.2	8.9	2.4
Serine	−33.5	5.2	−23.8	3.7	−28.0	4.0	−46.3	11.1
Threonine	−9.2	3.8	−2.2	2.0	8.4	2.2	−2.2	2.0
Valine	−15.6	3.6	−15.4	2.2	−4.4	3.2	−6.0	4.4

Note: Fluxes were calculated using the measured cell growth rates and the metabolite concentrations from 12 to 36 hr. Negative values represent consumption rates and positive values represent production rates.

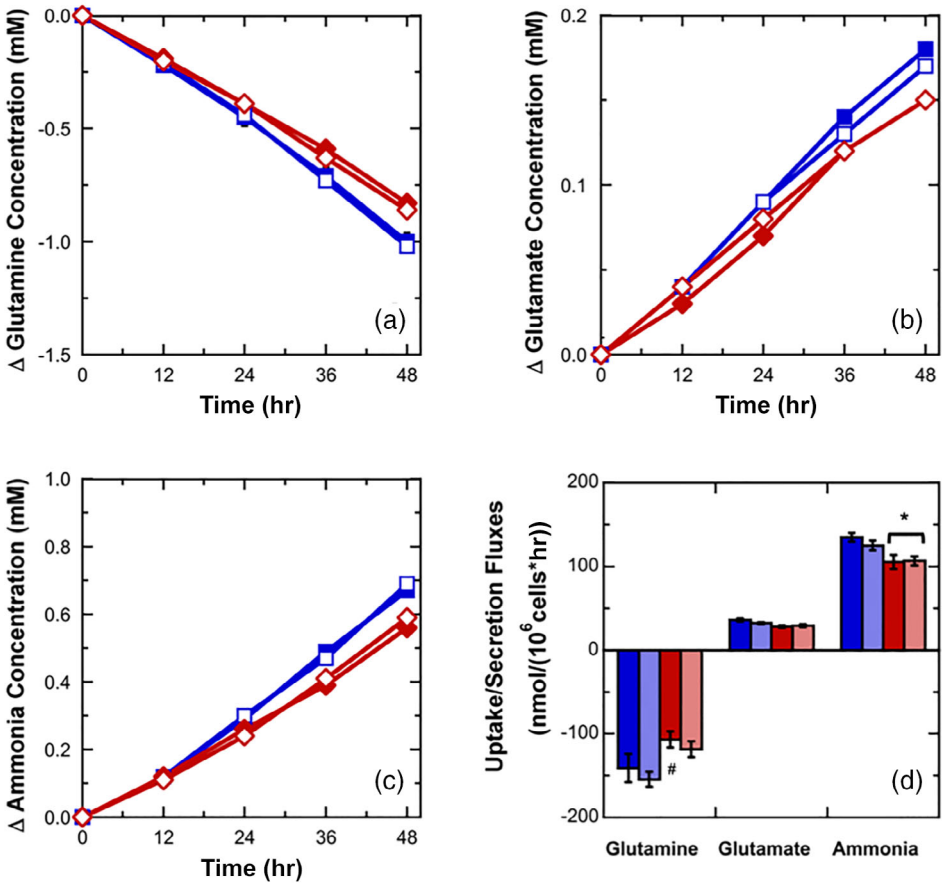

FIGURE 3 Glutamine consumption, glutamate production, and ammonia production profiles for K3 iPSCs. (a) Net glutamine consumption. (b) Net glutamate production. (c) Net ammonia production. (d) Calculated glutamine consumption, glutamate production, and ammonia production fluxes from 12 to 36 hr. Line graphs: Control media—blue square filled; Low Glucose media—blue square open; High Lactate media—red diamond filled; and Low Glucose + High Lactate—red diamond open. Bar graph: Control (blue), Low Glucose (light blue), High Lactate (red), and Low Glucose + High Lactate (light red). The asterisk (*) indicates the calculated flux was significantly different from the control condition ($p \leq .05$). The pound (#) indicates the calculated flux was significantly different from the low glucose condition ($p \leq .05$). Error bars represent *SE*s

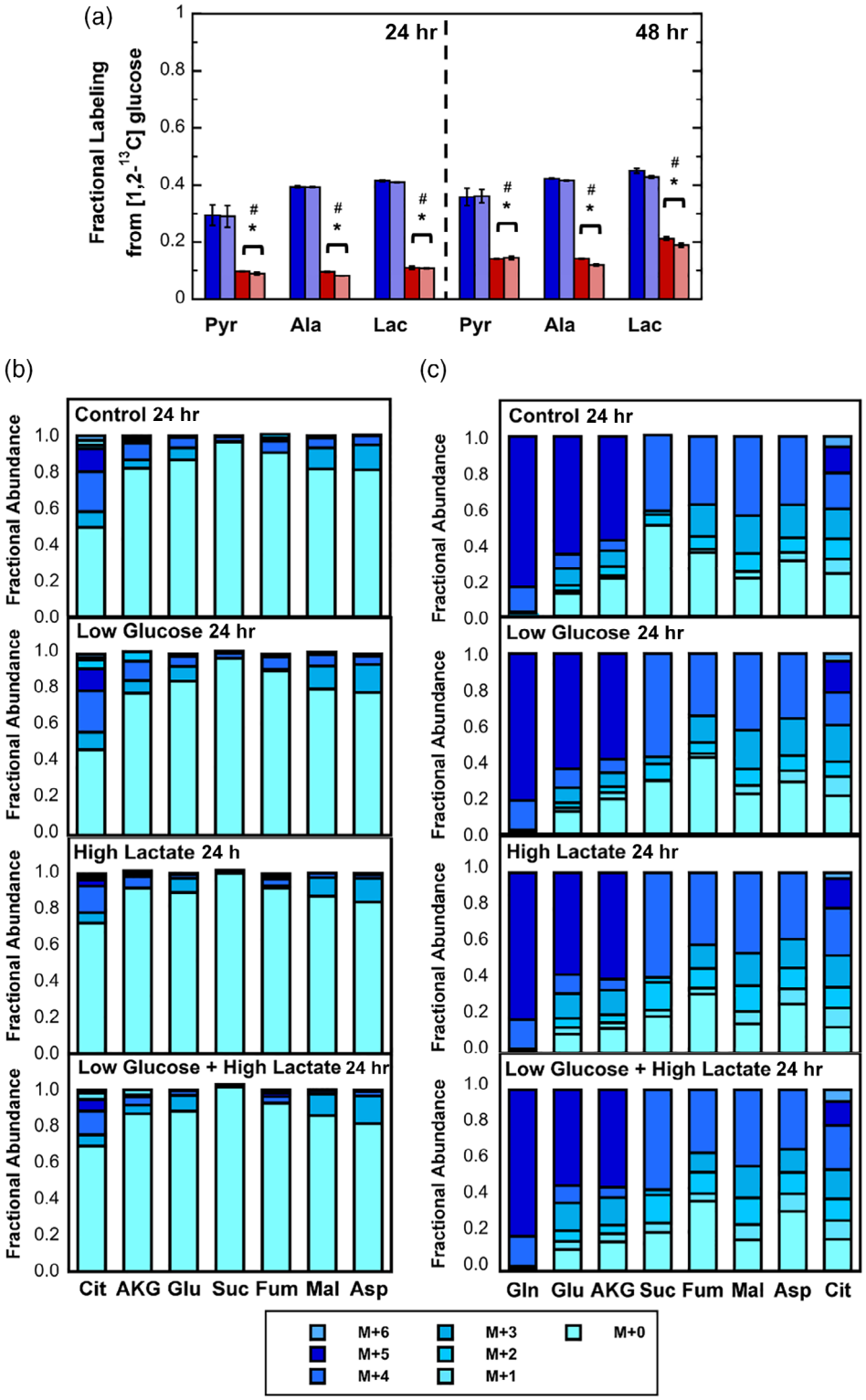

FIGURE 4 Fractional abundance due to isotopomer labeling for K3 iPSCs. (a) Pyruvate (Pyr), alanine (Ala), and lactate (Lac) from [1,2-$^{13}C_2$] glucose. (b) TCA metabolites from [1,2-$^{13}C_2$] glucose. (c) TCA metabolites from [U-$^{13}C_5$] glutamine. Citrate (Cit), α-ketoglutarate (AKG), glutamate (Glu), succinate (Suc), fumarate (Fum), malate (Mal), and aspartate (Asp), and glutamine (Gln). Control (blue), Low Glucose (light blue), High Lactate (red), and Low Glucose + High Lactate (light red) culture conditions. The metabolites are listed according to the order of oxidative TCA cycle. The asterisk (*) indicates the calculated flux was significantly different from the control condition ($p \leq .05$). The pound (#) indicates the calculated flux was significantly different from the low glucose condition ($p \leq .05$). Error bars represent *SE*s. The mass isotopomer distributions were corrected for natural abundances

3.3 | Intracellular metabolite labeling dynamics using [1,2-$^{13}C_2$] glucose tracer

To resolve glucose metabolism in the iPSC cultures, [1,2-$^{13}C_2$] glucose was used. This tracer has been previously identified as an excellent glucose tracer for resolving metabolic fluxes through glycolysis and the PPP for mammalian cells.[61] Intracellular MIDs were measured for pyruvate, alanine, and lactate from glucose tracer. In this study, poor resolution of the glycolytic metabolites—dihydroxyacetone phosphate, 3-phosphoglycerate, and phosphoenolpyruvate—were obtained; thus, these MIDs were not used in the subsequent model. Steady-state isotope labeling has previously been shown to occur within 24 hr for mammalian cells with similar growth rates.[37,61] The steady-state fractional labeling for pyruvate, alanine, and lactate are shown in Figure 4.

The fractional labeling for pyruvate, alanine, and lactate from glucose were lower for the high lactate cultures compared to cultures without added lactate. These results suggest that less glucose-derived carbon was metabolized to pyruvate, lactate, and alanine when lactate levels were high ($p \leq 0.05$). In contrast, the glucose concentration did not significantly affect the fractional labeling for these three species ($p > 0.05$). The fractional labeled species in glycolysis and measured glucose consumption fluxes are consistent with respect to the effects of the lactate concentration and glucose concentration (Figure 2f).

In addition to providing overall metabolite enrichment, [1,2-$^{13}C_2$] glucose was used to determine the distribution of mass isotopomers for intracellular metabolites. The MIDs for pyruvate, alanine and lactate from [1,2-$^{13}C_2$] glucose tracer at 24 and 48 hr for each culture condition are shown in Appendix G, Figure G1. Each metabolite was primarily unlabeled (M + 0) and M + 2 labeled. The predominant presence of M + 2 labeling, compared to M + 1 and M + 3, suggests that glycolysis was highly active in all four culture conditions. Also, the small fractional abundance of M1 labeling (>2% in each condition) suggests that the oxidative PPP was relatively inactive during exponential growth for each culture condition.

The fractional labeling of TCA metabolites from [1,2-$^{13}C_2$] glucose at 24 hr are shown in Figure 6a. The fractional labeling of citrate was lower for the high lactate cultures, as shown by the higher M + 0 fractional abundance. Additionally, the α-ketoglutarate (AKG) labeling from [1,2-$^{13}C_2$] glucose was also lower for the high lactate cultures. Together with the overall labeling, fractional abundance of M + 2 labeled citrate was lower for the high lactate cultures. These results indicate that glucose-derived carbon entered the TCA cycle either as ^{13}C-labeled acetyl-CoA via the enzyme pyruvate dehydrogenase (PDH) or as ^{13}C-labeled oxaloacetate via the enzyme pyruvate carboxylase (PC). Moreover, the decreased overall labeling, in particular M + 2 labeled TCA metabolites, suggests that glucose either served less as a carbon source for mitochondrial metabolism for both of the high lactate cultures, or glucose-derived ^{13}C labeling was diluted by catabolism of another unlabeled carbon substrate.

Lactate accumulation has previously been reported to reduce glycolytic activity by inhibiting hexokinase (HK) and phosphofructokinase (PFK) activity in mammalian cells, where lactate acts as a signaling molecule to down-regulate PFK activity.[62-65] In addition, lactate supplementation and conversion to pyruvate impairs NAD^+ generation and promotes pyruvate conversion to acetyl-CoA and entry into the TCA cycle; this also results in repressed glycolytic fluxes due to an increase in NADH/NAD^+ ratio.[54,66,67] The presence of ^{13}C-labeled TCA metabolites from the [1,2-$^{13}C_2$] glucose tracer confirm that some glucose-derived carbon supported oxidative mitochondrial metabolism rather than being used to generate lactate. Furthermore, the detection of significant intracellular citrate labeling from [1,2-$^{13}C_2$] glucose and the low AKG fractional labeling relative to citrate denotes that glucose catabolism supported acetyl-CoA synthesis (Figure 4b). These results are consistent with recent findings which determined that PSCs relied on a modified Warburg effect, where glucose can be converted to lactate and acetyl-CoA for PSC proliferation.[10,51]

3.4 | Intracellular metabolite labeling dynamics from [U-^{13}C] glutamine tracer

To resolve metabolism through the TCA cycle, [U-$^{13}C_5$] glutamine was used in parallel with the glucose tracer. The [U-$^{13}C_5$] glutamine has previously been shown to be the optimal glutamine tracer for rapidly labeling TCA cycle metabolites and for resolving metabolic fluxes through the TCA cycle for mammalian cells.[61] Figure 4c shows the fractional labeling of TCA cycle metabolites from [U-$^{13}C_5$] glutamine at 24 hr. [U-$^{13}C_5$] glutamine significantly labeled intracellular TCA cycle intermediate metabolites for all four culture conditions, with over 50% isotope labeling for all measured species (Figure 4c and Appendix G, Figure G3). In contrast, pyruvate, alanine, and lactate were minimally labeled from [U-$^{13}C_5$] glutamine (data in Appendix F, Table F2). The results suggest that glutamine is not a major carbon source for pyruvate and its byproducts. The overall intracellular metabolite labeling from [U-$^{13}C_5$] glutamine was similar for all four conditions; however, there were differences in fractional labeling of TCA metabolites. Overall, these results indicate that for iPSCs, glutamine serves integral anaplerotic role in TCA cycle metabolism, but has little role in pyruvate synthesis, regardless of the extracellular glucose and lactate concentrations investigated in this study (Figure 4c).

K3 iPSCs utilized reductive glutamine metabolism, irrespective of the glucose or lactate media concentration, as illustrated by the presence of M + 5 labeled citrate, along with M + 3 malate, fumarate, and aspartate (Figure 5a). Figure 5b outlines the reaction pathway for reductive carboxylation, including the labeling patterns. These results indicate that the reductive carboxylation appears to be slightly lower for the high lactate cultures; however, this observation is only significant when compared to the low glucose cultures ($p \leq 0.05$). These results demonstrate that glutamine was reductively metabolized through isocitrate dehydrogenase and ATP-citrate lyase (ACL) for lipid production in each culture. Reductive carboxylation of glutamine for lipid synthesis has previously been observed in cancer cells grown under hypoxic conditions (≤5% O_2)[38,39,61,66,68-70]; however, recently it has also been shown that mammalian cells employed reductive carboxylation in response to cell culture stress and due to various media formulations.[38,41] Further, hESCs have been shown to utilize glutamine-mediated reductive carboxylation in chemically defined media—E8 media.[51] Similarly, the results from this study indicate that iPSCs used reductive glutamine metabolism to support proliferation in chemically defined media under normoxic (20% O_2) conditions.

Interestingly, high lactate in the media also resulted in significantly higher M + 4 citrate, M + 3 AKG and glutamate, and M + 2 succinate, fumarate, malate, and aspartate labeling from [U-$^{13}C_5$] glutamine ($p \leq 0.05$) as shown in Figure 5c. These changes in intracellular TCA cycle metabolite labeling suggest elevated oxidative glutamine metabolism and retention of glutamine-derived carbon from multiple turns through the TCA cycle for the two high lactate culture conditions (Figure 5d). Interestingly, while glutamine consumption diminished for both of the high lactate culture conditions, it appears that the cells compensated for this by retaining more glutamine-derived carbon through multiple rounds of oxidative TCA cycle

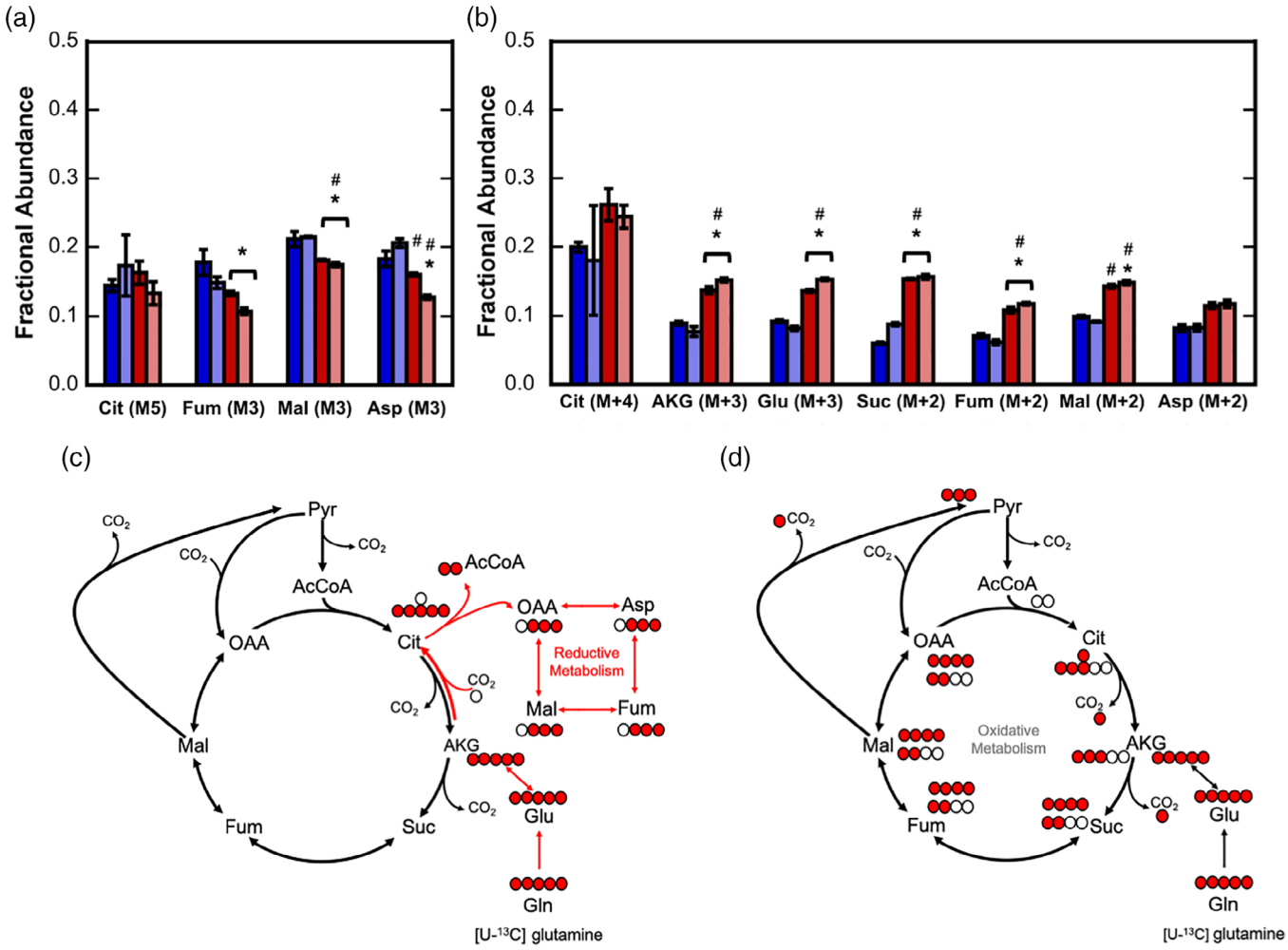

FIGURE 5 Fractional abundance of oxidative and reductive glutamine metabolite species from [U-$^{13}C_5$] glutamine at 24 hr. (a) Fractional abundance of M+5 citrate (Cit) and M+3 fumarate (Fum), malate (Mal), and aspartate (Asp). (b) Carbon atom transition for TCA metabolites from [U-13C5] glutamine. Red lines depict reductive glutamine metabolism that results in M+5 citrate (Cit) and M+3 oxaloacetate (OAA), malate (Mal), fumarate (Fum), and aspartate (Asp). (c) Fractional labeling of TCA cycle metabolites. (d) Potential mechanisms which would result in changes to fractional labeling of TCA cycle metabolites. The black lines depict oxidative glutamine metabolism that results in M+4 citrate (Cit), M+3 α-ketoglutarate (AKG) and glutamate (Glu), and M+2 succinate (Suc), fumarate (Fum), malate (Mal), and aspartate (Asp). Control media—blue; Low Glucose media—light blue; High Lactate media—red; and Low Glucose + High Lactate—light red. The metabolites are listed according to the order of oxidative TCA cycle. Red circles represent 13C and white 12C. The asterisk (*) indicates the fractional labeling was significantly different from the Control cultures ($p \leq .05$). The pound (#) indicates the fractional label was significantly different from the Low Glucose cultures ($p \leq .05$). MIDs were corrected for natural abundances. Error bars represent *SE*s

metabolism. Glutamine oxidation has previously been shown to be indispensable to hPSC metabolism and survival.[71] Also, elevated oxidative glutamine metabolism has previously been shown to occur for PSCs cultured in chemically defined media.[51] Similarly, lung carcinoma cells (A549) and osteosarcoma cells (143B) demonstrated increased oxidative glutamine metabolism in response to of 25 mM lactate supplementation, as seen by elevated M + 3 AKG and decreased reductive glutamine contribution to citrate.[66] Overall, in this study, K3 iPSCs relied primarily on oxidative glutamine metabolism to support proliferation, where the high lactate cultures had higher retention of glutamine-derived carbon through multiple rounds of oxidative TCA cycle metabolism.

3.5 | Intracellular metabolite labeling dynamics from [U-$^{13}C_3$] lactate tracer

To further understand the role of lactate as a potential metabolic substrate in iPSC metabolism, iPSCs were cultured with high extracellular lactate. [U-$^{13}C_3$] lactate was used to allow detection of lactate transport into the cell and metabolic conversion within the cell via MIDs of intracellular species. The amount of time required to reach isotopic steady-state from [U-$^{13}C_3$] lactate has not previously been reported for mammalian cells in glucose containing media, so the 24 and 48 hr timepoints were used to evaluate the intracellular lactate labeling dynamics throughout this experiment. Labeled intracellular

metabolites [U-$^{13}C_3$] lactate included: lactate, pyruvate, alanine, citrate, AKG, succinate, fumarate, malate, and aspartate. For both high lactate culture conditions, the fraction of labeled intracellular pyruvate, alanine, and lactate from [U-$^{13}C_3$] lactate was observed to be relatively constant between the 24 and 48 hr samples (Figure 6a,b). The pyruvate, alanine, and lactate were primarily M + 3 labeled. As shown in Figure 6c, [U-$^{13}C_3$] lactate transport across the cell membrane and direct conversion to pyruvate and alanine results in M + 3 labeling. There was also observed M + 2 labeling of pyruvate after 24 hr, which requires TCA cycle metabolism and conversion to pyruvate via malic enzyme (ME) activity. Figure 6d,e illustrate the mechanisms to generate M + 2 pyruvate.

For the TCA cycle metabolites, citrate was highly labeled at 24 hr for both high lactate cultures, whereas AKG, malate, and aspartate were all significantly less labeled, as illustrated by the fractional abundance of M + 0 in each metabolite (Figure 7). Succinate and fumarate were also less labeled than citrate. Succinate and fumarate labeling were lower due to significant dilution from consumption of unlabeled amino acids. As mentioned above, M + 2 pyruvate labeling was observed from [U-$^{13}C_3$] lactate after 24 hr of culture; this would result from metabolism of [U-$^{13}C_3$] lactate through one round of the TCA cycle and converted back to pyruvate through ME activity. ^{13}C-lactate can enter into the TCA cycle either through PDH or PC reactions. While metabolism of ^{13}C-lactate through each of these reactions would result in M + 2 labeling of pyruvate, as illustrated in Figure 6d (PDH) and Figure 6e (PC), each pathway would result in differential citrate labeling. The higher fractional abundance of M + 2 citrate compared to M + 3 would suggest that the PDH reaction was more active in metabolism of ^{13}C-lactate into the mitochondria.

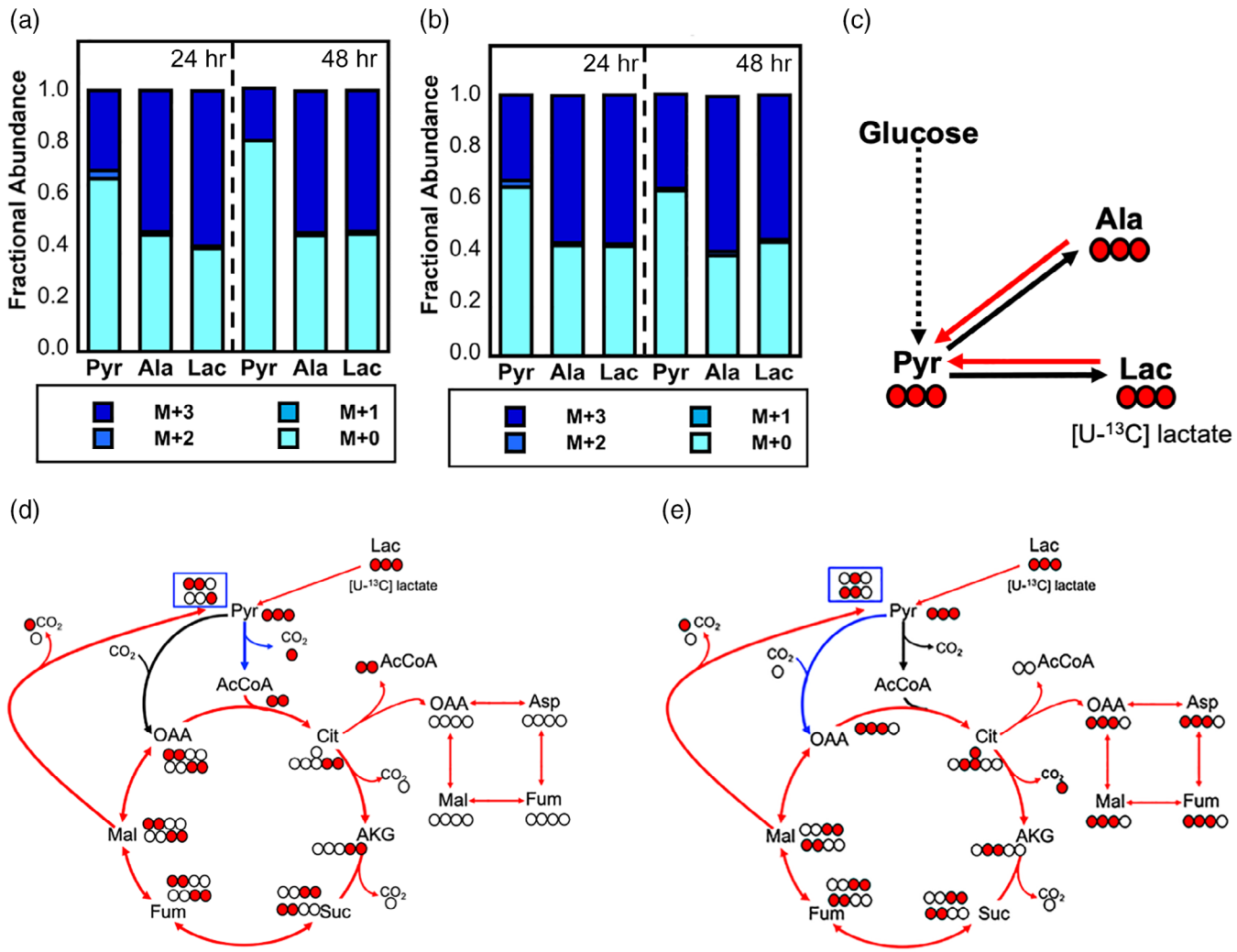

FIGURE 6 Fractional abundance for glycolytic metabolites and potential mechanisms for generating M + 2 labeled pyruvate from [U-$^{13}C_3$] lactate labeling. (a) High Lactate media. (b) Low Glucose + High Lactate media. (c) Carbon atom transition for glycolytic metabolites from [U-$^{13}C_3$] lactate. (d) Pyruvate conversion to acetyl-CoA via the pyruvate dehydrogenase (PDH) enzyme. (e) Pyruvate carboxylation to oxaloacetate via the pyruvate carboxylase (PC) enzyme. Pyruvate (Pyr), alanine (Ala), and lactate (Lac) metabolites are shown. Red circles represent ^{13}C and white ^{12}C. Red lines indicate lactate consumption and metabolism to intracellular pyruvate and alanine. Black lines represent production of alanine and lactate from glucose. The blue lines represent the two reactions responsible for entry of M + 3 pyruvate into the TCA cycle. MIDs were corrected for natural abundances

Interestingly, fractional intracellular labeling from ^{13}C-lactate remained relatively constant between 24 and 48 hr for glycolytic byproducts (Figure 6a,b), while in contrast, the fractional labeling of the TCA cycle metabolites was significantly higher at 48 hr, as shown in Figure 7 and in Appendix G, Figure G4. These results suggest that [U-$^{13}C_3$] lactate labeling of intracellular alanine, lactate, and pyruvate reached isotopic steady-state by 24 hr, while the TCA cycle metabolites had not yet approached isotopic steady-state. Also, along with the decreased contribution of [1,2-$^{13}C_2$] glucose to pyruvate and TCA cycle metabolism for the two high lactate cultures, the uptake and metabolism of the [U-$^{13}C_3$] lactate tracer implies that the conversion of lactate to pyruvate is rapid relative to glucose catabolism and that lactate contributed as a carbon source for iPSC metabolism. A similar metabolic response was observed for various types of cancer cells cultured in high lactate supplemented media.[66] It is widely accepted that cancer cells are capable of consuming and metabolizing lactate as a metabolic substrate.[15,16,18,72] Similarly, these results indicate that ^{13}C-lactate was continuously in exchange across the cell membrane and served as a metabolic substrate to support K3 iPSC proliferation throughout exponential growth.

The high fractional abundance of labeled citrate relative to other TCA metabolites also suggests that lactate served as a substrate in support of lipid synthesis. Proliferative cells perform de novo lipid synthesis rather than scavenging for free fatty acids, which results in truncated TCA cycle metabolism, with high ACL activity to support lipid synthesis; this results in citrate and acetyl-CoA primarily supporting lipid synthesis.[4,51] Lactate-derived carbon supported lipid synthesis and histone acetylation in cancer cell metabolism.[16,73] Specifically, cells exposed to 10 mM extracellular lactate exhibited increased histone acetylation for a breast cancer cell line and increased malignancy and stemness gene expression.[16] Further, in an in vivo human lung tumor model, lactate preferentially supported mitochondrial metabolism over glucose.[74] Similarly, acetyl-CoA production has been shown to be critical for the maintenance of PSCs, where decreased glycolytic flux and decreased acetyl-CoA production can result in the onset of spontaneous differentiation; however, acetate media supplementation prevented early spontaneous differentiation.[10] Moreover, inhibition of PDH kinase, a PDH inhibitor, redirected glucose-derived carbon to acetyl-CoA rather than lactate and resulted in increased histone acetylation and a higher percentage of Oct4 positive cells.[10] In a similar manner, lactate appears to support

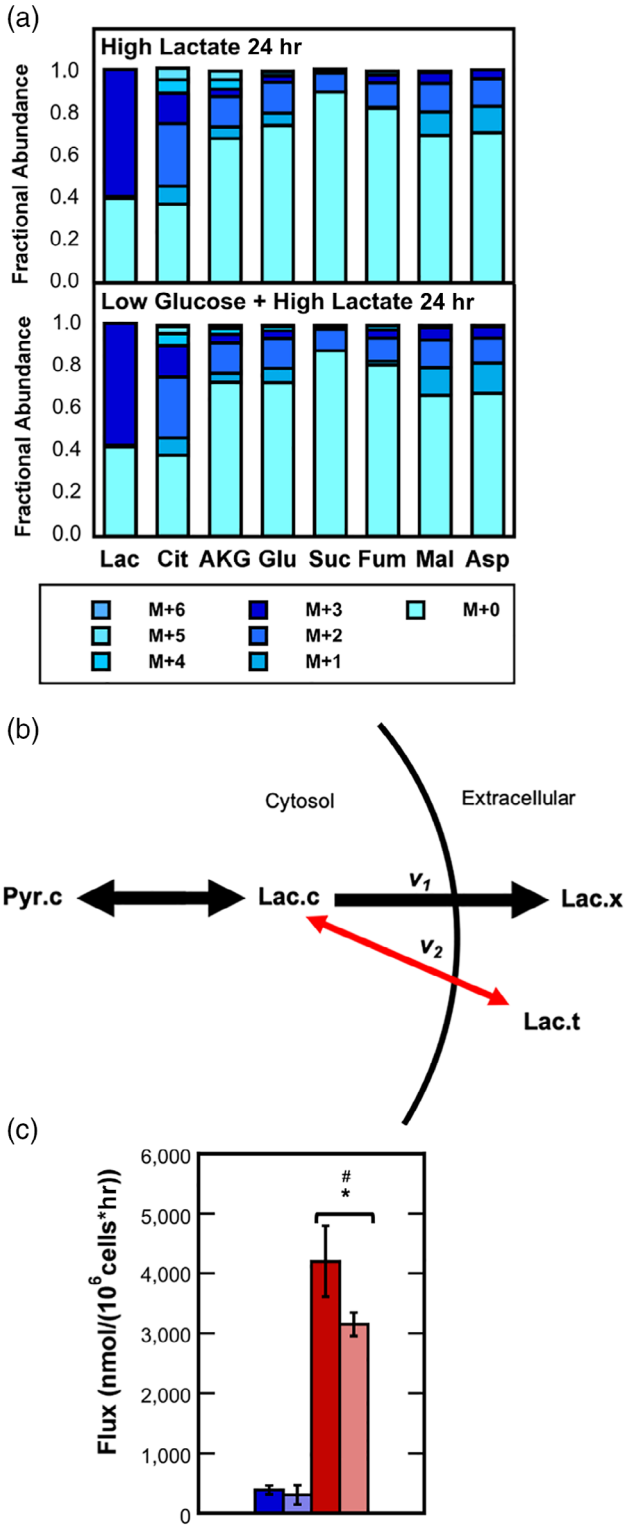

FIGURE 7 Legend on next page.

FIGURE 7 Uptake of [U-$^{13}C_3$] lactate labeling by K3 iPSCs. (a) Fractional abundance of ^{13}C mass isotopomer distributions for TCA metabolites from High Lactate and Low Glucose + High Lactate cultures. TCA metabolites represented are citrate (Cit), α-ketoglutarate (AKG), glutamate (Glu), succinate (Suc), fumarate (Fum), malate (Mal), and aspartate (Asp). (b) A diagram of the metabolic reactions used to model lactate production and lactate consumption for K3 iPSCs using ^{13}C-MFA. Reaction v1 represents the net lactate production flux. Reaction v2 represents the reversible flux of lactate tracer into and out of the cell. (c) Simulated lactate tracer exchange flux in Control media—blue; Low Glucose media—light blue; High Lactate media—red; and Low Glucose + High Lactate—light red culture media. The asterisk (*) indicates the flux was significantly different from the control condition ($p \leq .05$). The pound (#) flux was significantly different from the low glucose condition ($p \leq .05$). Error bars represent *SE*. The mass isotopomer distributions were corrected for natural abundances

K3 iPSC mitochondrial metabolism without impacting cell proliferation at the concentrations examined.

3.6 | Pluripotency

In order to determine the effects of the glucose and lactate concentrations on iPSC pluripotency, K3 iPSCs were grown for one and five passages under each culture condition. Cells from these cultures were analyzed for pluripotency gene expression using qPCR and protein expression by western blot analysis. Three genes were used to monitor pluripotency—Oct4, Sox2, and Nanog.[75] Oct4 expression was selected to assess pluripotency by protein expression via western blots. The gene expression levels for Oct4, Sox2, and Nanog are shown in Figure 8a,c for K3 iPSCs cultured for one or five passages in the four culture media. For the cultures after one passage, none of the genes had significantly different expression ($p > 0.05$). Sox2 and Nanog expression levels were significantly higher for the five passage low glucose + high lactate cultures ($p \leq 0.05$); however, glucose and lactate media concentrations did not affect Oct4 gene expression levels after five passages ($p > 0.05$) (Figure 8c). Also, normalized Oct4 protein expression levels were similar for all four cultures after one and five passages in each culture condition ($p > 0.05$) (Figure 8b,d).

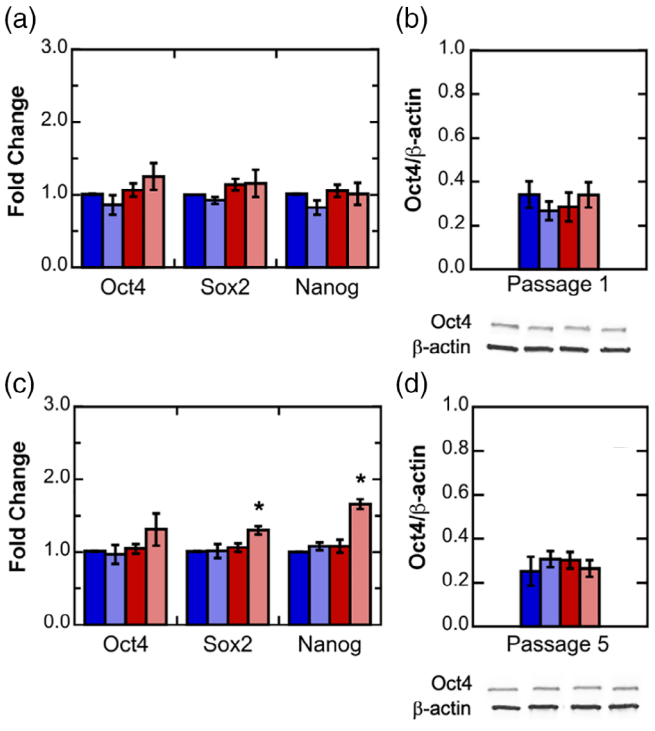

FIGURE 8 Comparison of pluripotency gene and protein expression for K3 iPSCs after one and five passages under different initial glucose and lactate concentrations. (a) Normalized gene expression after 1-passage for Oct4, Sox2, and Nanog. (b) Normalized protein expression after 1-passage for Oct4. (c) Normalized gene expression after 5-passages for Oct4, Sox2, and Nanog. (d) Normalized protein expression after 5-passages for Oct4. Control media—blue; Low Glucose media—light blue; High Lactate media—red; and Low Glucose + High Lactate—light red. The asterisk (*) indicates that the normalized gene or protein expressions were significantly different from the control ($p \leq .05$). Error bars represent *SE*

Tight regulation of Oct4 expression is required to maintain pluripotency for PSCs in vitro. Elevated Oct4 expression has been shown to induce differentiation towards the primitive ectoderm and mesoderm, while loss of Oct4 expression caused differentiation towards the trophectoderm.[76,77] Sox2 expression must be also tightly regulated to maintain pluripotency. Loss of Sox2 expression induces differentiation towards the trophectoderm.[78] In addition, a two- to five-fold increase in Sox2 expression resulted in differentiation towards the trophectoderm and loss of Oct4 and Nanog expression.[79] Similarly, Nanog expression represses differentiation towards the primitive ectoderm.[80] However, overexpression of Nanog also prevented differentiation in ESCs.[76] Interestingly, Oct4 serves as a transcriptional regulator for HK and PFK—two key glycolytic enzymes—and maintenance of Oct4 expression and elevated glycolytic fluxes are critical factors for maintaining iPSC pluripotency.[81] In this study, the observed decreased glucose consumption due to high lactate did not affect Oct4 expression. Thus, the reduced glucose catabolism appears to have resulted from high lactate exposure alone, rather than loss of Oct4 expression. In previous work, high lactate concentrations have been shown to have variable effects on PSC pluripotency; murine ESCs and iPSCs proliferated and maintained pluripotency in lactate concentrations up to 40 mM, while hESCs exhibited decreased pluripotency through Tra-1-60 expression after continuous passaging in 22 mM lactate containing media.[16,19,52,53] The results of this study suggest that glucose and lactate concentrations within ranges that support equal exponential growth do not negatively affect human K3 iPSC pluripotency.

3.7 | Metabolic flux analysis

Detailed intracellular metabolic fluxes were generated for the four culture conditions using the parallel ^{13}C-labeling data, the extracellular measured fluxes, and the metabolic network. The parallel labeling data used in the MFA model included the [1,2-$^{13}C_2$] glucose and [U-$^{13}C_5$] glutamine MIDs for all culture conditions and the [U-$^{13}C_3$] lactate MIDs for the high lactate culture conditions. As previously mentioned, the [U-$^{13}C_3$] lactate tracer provided evidence that lactate was consumed and metabolized by K3 iPSCs in both high lactate cultures (Figure 7); however, net lactate production was observed for K3 iPSCs in all four culture conditions (Figure 2). Thus, lactate was produced and consumed by iPSCs in the high lactate cultures. While the metabolic contribution of circulating lactate has previous been studied in vivo, to our knowledge, no one has previously used ^{13}C-MFA to model the dual consumption and production of lactate in vitro with an isotopically labeled tracer.[74,82] Therefore, a novel approach was employed to model the reversible metabolism of the lactate tracer in this study.

The metabolic reaction scheme used to model lactate production and consumption is shown in Figure 7a, where reaction v_1 represents

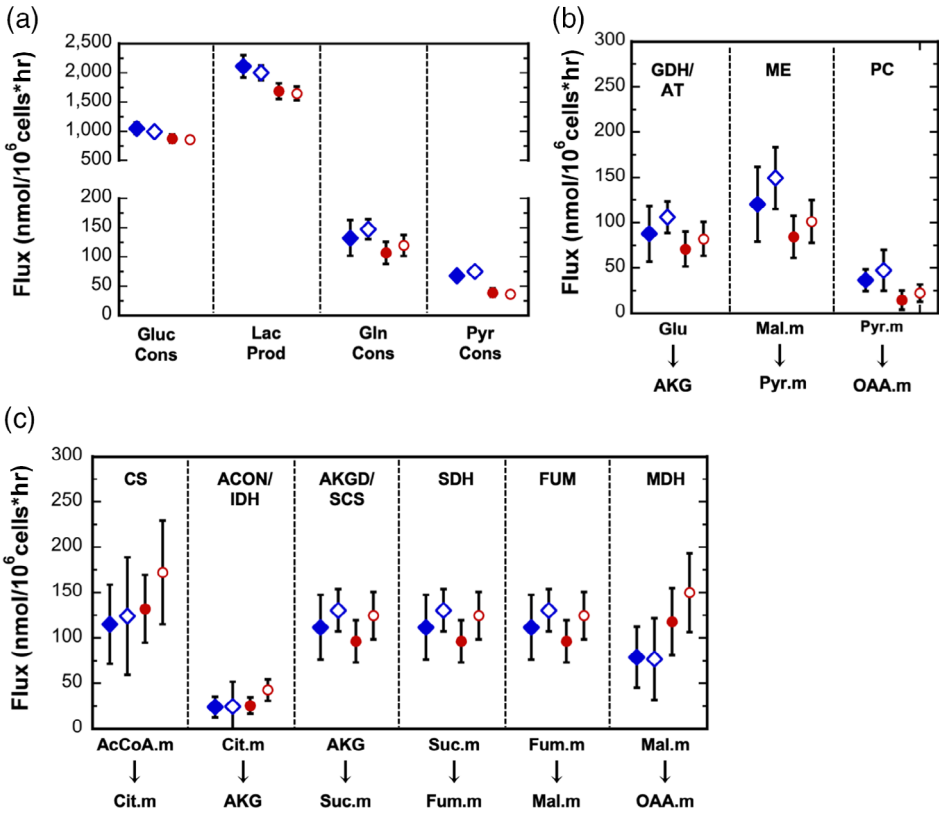

FIGURE 9 Comparison of simulated metabolic fluxes from ^{13}C-MFA for K3 iPSCs. (a) Key extracellular uptake and secretion rates. (b) Anaplerotic fluxes. (c). TCA cycle metabolic fluxes. Control media—blue diamond filled; Low Glucose media—blue diamond open; High Lactate media—red circle filled; and Low Glucose + High Lactate—red circle open. Error bars represent 95% confidence intervals. ACON/IDH, aconitase/isocitrate dehydrogenase; AKGD/SCS, AKG dehydrogenase/ succinyl coenzyme A synthetase; CS, citrate synthase; FUM, fumarase; GDH/AT, glutamate dehydrogenase/ aminotransferase; MDH, malate dehydrogenase; ME, malic enzyme; PC, pyruvate carboxylase; SDH, succinate dehydrogenase

the measured net production flux of lactate from the cytosol (Lac.c) to the extracellular media (Lac.x), and reaction v_2 represents the consumption flux of lactate tracer (Lac.t) into the cytosol (Lac.c). The magnitude of the lactate tracer flux was not measured; thus, the lactate tracer flux could not be constrained to a known measurement. Instead, the lactate tracer reaction into the cell was defined as a reversible reaction and fixed to a net flux of zero. This allowed for the model to simulate an infinite exchange of the lactate tracer into and out of the cell without defining a net lactate tracer flux. The model predicted net lactate production fluxes for all four culture conditions. Also, lactate tracer exchange fluxes into the cell were also simulated in all four conditions, with the model predicting approximately 10 times higher lactate exchange fluxes for both of the high lactate culture conditions (Figure 7b). These results indicate that the metabolic model was capable of incorporating [U-$^{13}C_3$] lactate tracer into the cell even though a net lactate production flux was observed. Previously, Brodsky et al. (2019) used [U-$^{13}C_3$] lactate tracer along with ^{13}C-MFA to determine the contribution of lactate to breast cancer metabolism; however, intracellular metabolite labeling from [U-$^{13}C_3$] lactate tracer was not incorporated in the ^{13}C-MFA simulations, in part due to much lower intracellular labeling due to lactate. The metabolic network reactions used in this work allowed for [U-$^{13}C_3$] lactate MIDs to be incorporated into the ^{13}C-MFA simulations to account for consumption of lactate tracer. Additionally, this basic reaction scheme could be used to allow other waste metabolites to be labeled and incorporated into the MFA models.

The intracellular metabolic flux distributions from ^{13}C-MFA simulations for K3 iPSCs from all four culture conditions are shown graphically on the metabolic maps shown in Appendix J, Figures J1. As expected, the glucose consumption and lactate production rates had the highest fluxes in each condition. Additionally, the simulations predicted lower glucose consumption and lactate production fluxes for the two high lactate culture conditions compared to the control and low glucose cultures (Figure 9a). In order for the model to converge to an acceptable fit for each culture condition, a fatty acid sink (FA.snk) reaction was included in the model. Sink reactions have previously been used to account for loss of carbon through metabolic reactions not included in the metabolic network model. Recently, PSCs have been shown to possess some metabolic flexibility in response to media formulations, especially with regards to acetyl-CoA generation and lipid biosynthesis rates.[10,51] Since lipid content was not measured in this study, the fatty acid sink flux allowed for flexibility with respect to lipid biosynthesis predictions. Interestingly, the model predicted higher fluxes to the fatty acid sink for each of the high lactate cultures (Figures 9a–d). Along with the high fractional labeling of citrate from [U-$^{13}C_3$] lactate, these metabolic flux simulations indicate that lactate supplementation promoted acetyl-CoA production and lipid biosynthesis in each of the high lactate culture conditions.

Similar to the extracellular concentration measurements, the metabolic flux model simulated lower glutamine consumption fluxes, as well as reduced conversion of glutamine to AKG. As a result, slightly lower fluxes through the TCA cycle were also predicted, as illustrated by consistent citrate synthase (CS), α-ketoglutarate dehydrogenase (AKGD), succinate dehydrogenase (SDH), and fumarase (FUM) fluxes (Figure 9c). The metabolic flux models also predicted high ME activity for the iPSCs in all four culture conditions (Figure 9b). However,

glutaminolysis was not the major source of pyruvate production, with ME fluxes approximately 10% of the glucose consumption fluxes. Interestingly, the metabolic model predicted lower ME fluxes for the two high lactate conditions (Figure 9b); this also corresponded with decreased simulated flux from pyruvate to oxaloacetate through PC. This indicates a lower anaplerotic contribution of glutamine to mitochondrial pyruvate via ME due to high extracellular lactate. Elevated cycling between ME and PC has previously been observed for Chinese hamster ovary (CHO) cells and was suggested to be the cause for low oxidative PPP fluxes during early exponential growth, since the NADP-dependent isoform of ME can provide NADPH to meet cellular demands.[47,83] Also, oxidative glutaminolysis to pyruvate through ME served as a significant source of NADPH for glioma cells.[84]

As mentioned earlier, the increased M + 3 AKG and glutamate labeling, and M + 2 succinate, fumarate, malate, and aspartate labeling from [U-$^{13}C_5$] glutamine in the high lactate cultures represents increased oxidative glutamine metabolism and higher retention of ^{13}C-labeled metabolites in the TCA. This was also coupled with increased malate dehydrogenase activity in the high lactate cultures, as illustrated by increased flux of oxaloacetate to malate in the cytosol and increased flux of malate to oxaloacetate in the mitochondria (Figure 9). Along with this, increased malate transport from the cytosol to the mitochondria was predicted. These results suggest increased malate–aspartate shuttle activity in the high lactate culture conditions. The malate–aspartate shuttle is responsible for transporting reducing cofactors from the cytosol to the mitochondria.[85] Since lactate was metabolized to pyruvate in the high lactate cultures, this would result in elevated cytosolic NADH production. Therefore, increased malate shuttle activity would support transport of reducing cofactors generated from lactate catabolism into the mitochondria for oxidative phosphorylation. These results illustrate an underlying metabolic flexibility of iPSCs in response to low glucose and high lactate culture conditions.

4 | CONCLUSIONS

In this study, the metabolic responses of K3 iPSCs to different glucose and lactate concentrations that range from normal to low for glucose and zero to high (20 mM) for lactate were examined using ^{13}C-MFA. Parallel labeling experiments were performed using ^{13}C-glucose, ^{13}C-glutamine, and ^{13}C-lactate to determine the contribution of each as metabolites to central carbon metabolism. [1,2-$^{13}C_2$] glucose and [U-$^{13}C_5$] glutamine were used to resolve intracellular fluxes through glycolysis and the TCA cycle. For the two high lactate culture conditions, the [U-$^{13}C_3$] lactate tracer was also used to investigate the metabolic contribution of lactate to iPSC metabolism. The metabolic network model constructed for iPSCs in this study was adapted from metabolic models constructed for CHO cells and for other mammalian cells, including cancer cells. The extracellular flux measurements and measured intracellular MIDs were coupled with a defined metabolic network to predict intracellular fluxes. Pluripotency of the K3 iPSCs were assessed by comparing gene and protein expression levels for cells cultured for one and five passages in each of the media.

While lactate is primarily viewed as a metabolic waste product in in vitro iPSC culture, the results from this study suggest that lactate accumulation alone does not adversely impact iPSC growth or pluripotency at the concentrations tested. Also, these results support the idea that media acidification, which results from lactate production, is potentially the root of the problem associated with continuous iPSC culture, rather than lactate alone. Therefore, as more iPSC culture processes move towards pH-controlled bioreactors, lactate accumulation could be controlled to improve iPSCs quality. In addition, since low glucose and high lactate growth media did not adversely impact iPSC proliferation or pluripotency, this indicates that implementation of fed-batch bioprocessing conditions for iPSCs is feasible in the future.

The findings in this study also illustrate that iPSCs possess metabolic flexibility with regards to lactate metabolism, which has not been previously reported. This flexibility allows for iPSCs to undergo distinct substrate utilization strategies to support self-renewal when cultured in a range of glucose and lactate concentrations. In rapidly proliferating cells, dual consumption of glucose and lactate could support replication and cell division since carbon from glucose and lactate can be compartmentalized to synthesize different biomass precursors. Since iPSCs are frequently cultured in 3D aggregates when grown in suspension, substrate availability depends on aggregate size and the proximity of cells to the aggregate surface. Metabolic flexibility would support proliferation of cells in different regions of a cell aggregate without adversely influencing pluripotency. The results from this study illustrate that K3 iPSCs possess the ability to metabolize lactate as a metabolic substrate to support cell proliferation and pluripotency maintenance, even in the presence of sufficient glucose. And finally, this work demonstrated that an alternative reaction scheme can be used to incorporate labeled waste products into a ^{13}C-MFA model, which opens up many avenues for exploration of cell metabolism.

ACKNOWLEDGMENTS

We would like to thank Paul Gulde and Serena Smith from Thermo Fisher Scientific for donating custom medium for this research. We would also like to thank Dr. Stephen A. Duncan at the Medical University of South Carolina for donating the K3 iPSCs. Finally, we would like to thank Drs. Feihn and Bei Gao at the West Coast Metabolomics Center at the University of California, Davis for conducting the GC–MS analysis.

AUTHOR CONTRIBUTIONS

Daniel Odenwelder: Conceptualization; formal analysis; investigation; methodology; writing-original draft; writing-review and editing. **Xiaoming Lu:** Data curation; formal analysis; investigation; methodology. **Sarah Harcum:** Conceptualization; data curation; formal analysis; funding acquisition; supervision; visualization; writing-original draft; writing-review and editing.

PEER REVIEW

The peer review history for this article is available at https://publons.com/publon/10.1002/btpr.3090.

DATA AVAILABILITY STATEMENT

The data that supports the findings of this study are available in the supplementary material of this article.

ORCID

Sarah W. Harcum https://orcid.org/0000-0001-9417-0489

REFERENCES

1. Gu W, Gaeta X, Sahakyan A, et al. Glycolytic metabolism plays a functional role in regulating human pluripotent stem cell state. *Cell Stem Cell*. 2016;19:476-490.
2. Varum S, Rodrigues AS, Moura MB, et al. Energy metabolism in human pluripotent stem cells and their differentiated counterparts. *Plos One*. 2011;6:15.
3. Zhang J, Khvorostov I, Hong JS, et al. UCP2 regulates energy metabolism and differentiation potential of human pluripotent stem cells. *EMBO J*. 2011;30:4860-4873.
4. DeBerardinis RJ, Lum JJ, Hatzivassiliou G, Thompson CB. The biology of cancer: metabolic reprogramming fuels cell growth and proliferation. *Cell Metab*. 2008;7:11-20.
5. Folmes CDL, Dzeja PP, Nelson TJ, Terzic A. Metabolic plasticity in stem cell homeostasis and differentiation. *Cell Stem Cell*. 2012;11:596-606.
6. Folmes CDL, Nelson TJ, Martinez-Fernandez A, et al. Somatic oxidative bioenergetics transitions into pluripotency-dependent glycolysis to facilitate nuclear reprogramming. *Cell Metab*. 2011;14:264-271.
7. Ryall JG, Cliff T, Dalton S, Sartorelli VJCSC. Metabolic reprogramming of stem cell epigenetics. *Cell Stem Cell*. 2015;17:651-662.
8. Ezashi T, Das P, Roberts RM. Low O-2 tensions and the prevention of differentiation of hES cells. *Proc Natl Acad Sci U S A*. 2005;102:4783-4788.
9. Mohyeldin A, Garzon-Muvdi T, Quinones-Hinojosa A. Oxygen in stem cell biology: a critical component of the stem cell niche. *Cell Stem Cell*. 2010;7:150-161.
10. Moussaieff A, Rouleau M, Kitsberg D, et al. Glycolysis-mediated changes in acetyl-CoA and histone acetylation control the early differentiation of embryonic stem cells. *Cell Metab*. 2015;21:392-402.
11. Cairns RA, Harris IS, Mak TW. Regulation of cancer cell metabolism. *Nat Rev Cancer*. 2011;11:85-95.
12. Vander Heiden MG, Cantley LC, Thompson CBJS. Understanding the Warburg effect: the metabolic requirements of. *Cell Prolif*. 2009;324:1029-1033.
13. Warburg O. On the origin of cancer cells. *Science*. 1956;123:309-314.
14. Kennedy KM, Dewhirst MW. Tumor metabolism of lactate: the influence and therapeutic potential for MCT and CD147 regulation. *Future Oncol*. 2010;6:127-148.
15. Kennedy KM, Scarbrough PM, Ribeiro A, et al. Catabolism of exogenous lactate reveals it as a legitimate metabolic substrate in breast cancer. *PLoS One*. 2013;8:20.
16. Martinez-Outschoorn UE, Prisco M, Ertel A, et al. Ketones and lactate increase cancer cell "stemness", driving recurrence, metastasis and poor clinical outcome in breast cancer. *Cell Cycle*. 2011;10:1271-1286.
17. Pavlides S, Tsirigos A, Vera I, et al. Loss of stromal caveolin-1 leads to oxidative stress, mimics hypoxia and drives inflammation in the tumor microenvironment, conferring the "reverse Warburg effect" a transcriptional informatics analysis with validation. *Cell Cycle*. 2010;9:2201-2219.
18. Sonveaux P, Vegran F, Schroeder T, et al. Targeting lactate-fueled respiration selectively kills hypoxic tumor cells in mice. *J Clin Investig*. 2008;118:3930-3942.
19. Chen XL, Chen A, Woo TL, Choo ABH, Reuveny S, Oh SKW. Investigations into the metabolism of two-dimensional Colony and suspended microcarrier cultures of human embryonic stem cells in serum-free media. *Stem Cells Dev*. 2010;19:1781-1792.
20. Nath SC, Nagamori E, Horie M, Kino-oka M. Culture medium refinement by dialysis for the expansion of human induced pluripotent stem cells in suspension culture. *Bioprocess Biosystems Eng*. 2017;40:123-131.
21. Ouyang A, Ng R, Yang ST. Long-term culturing of undifferentiated embryonic stem cells in conditioned media and three-dimensional fibrous matrices without extracellular matrix coating. *Stem Cells*. 2007;25:447-454.
22. Tohyama S, Hattori F, Sano M, et al. Distinct metabolic flow enables large-scale purification of mouse and human pluripotent stem cell-derived cardiomyocytes. *Cell Stem Cell*. 2013;12:127-137.
23. Olmer R, Lange A, Selzer S, et al. Suspension culture of human pluripotent stem cells in controlled, stirred bioreactors. *Tissue Eng Part C-Methods*. 2012;18:772-784.
24. Wang Y, Chou BK, Dowey S, He CX, Gerecht S, Cheng LZ. Scalable expansion of human induced pluripotent stem cells in the defined xeno-free E8 medium under adherent and suspension culture conditions. *Stem Cell Res*. 2013;11:1103-1116.
25. Stephanopoulos G. Metabolic fluxes and metabolic engineering. *Metab Eng*. 1999;1:1-11.
26. Bonarius HPJ, Schmid G, Tramper J. Flux analysis of underdetermined metabolic networks: the quest for the missing constraints. *Trends Biotechnol*. 1997;15:308-314.
27. Stephanopoulos G, Aristidou A, Nielsen J. *Metabolic Engineering: Principles and Methodologies*. San Diego: Academic Press; 1998.
28. Niklas J, Heinzle E. Metabolic flux analysis in systems biology of mammalian cells. *Genomics and Systems Biology of Mammalian Cell Culture*. Berlin: Springer-Verlag; 2011:109-132.
29. Sa JV, Duarte TM, Carrondo MJT, Alves PM, Teixeira AP. In: Al-Rubeai M, ed. *Animal Cell Culture*. Vol 9. Heidelberg: Springer; 2015:521-539.
30. Sauer U. Metabolic networks in motion: ^{13}C-based flux analysis. *Mol Syst Biol*. 2006;2:10.
31. Si-Tayeb K, Noto FK, Sepac A, et al. Generation of human induced pluripotent stem cells by simple transient transfection of plasmid DNA encoding reprogramming factors. *BMC Dev Biol*. 2010;10:10.
32. Nagaoka M, Si-Tayeb K, Akaike T, Duncan SA. Culture of human pluripotent stem cells using completely defined conditions on a recombinant E-cadherin substratum. *BMC Dev Biol*. 2010;10:12.
33. Watanabe K, Ueno M, Kamiya D, et al. A ROCK inhibitor permits survival of dissociated human embryonic stem cells. *Nat Biotechnol*. 2007;25:681-686.
34. Liu W, Ren Z, Lu K, et al. The suppression of medium acidosis improves the maintenance and differentiation of human pluripotent stem cells at high density in defined cell culture medium. *Int J Biol Sci*. 2018;14:485.
35. Badawy A-B, Morgan C, Turner J. Application of the Phenomenex EZ: faast™ amino acid analysis kit for rapid gas-chromatographic determination of concentrations of plasma tryptophan and its brain uptake competitors. *Amino Acids*. 2008;34:587-596.
36. Murphy TA, Young JD. ETA: robust software for determination of cell specific rates from extracellular time courses. *Biotechnol Bioeng*. 2013;110:1748-1758.
37. Ahn WS, Antoniewicz MR. Parallel labeling experiments with [1, 2-^{13}C] glucose and [U-^{13}C] glutamine provide new insights into CHO cell metabolism. *Metab Eng*. 2013;15:34-47.
38. Jiang L, Shestov AA, Swain P, et al. Reductive carboxylation supports redox homeostasis during anchorage-independent growth. *Nature*. 2016;532:255-258.
39. Metallo CM, Gameiro PA, Bell EL, et al. Reductive glutamine metabolism by IDH1 mediates lipogenesis under hypoxia. *Nature*. 2012;481:380-U166.

40. Bonarius HP, Hatzimanikatis V, Meesters KP, de Gooijer CD, Schmid G, Tramper J. Metabolic flux analysis of hybridoma cells in different culture media using mass balances. *Biotechnol Bioeng*. 1996;50: 299-318.
41. Brodsky AN, Odenwelder DC, Harcum SW. High extracellular lactate causes reductive carboxylation in breast tissue cell lines grown under normoxic conditions. *PloS One*. 2019;14:e0213419.
42. Young JD. INCA: a computational platform for isotopically nonstationary metabolic flux analysis. *Bioinformatics*. 2014;30:1333-1335.
43. Antoniewicz MR, Kelleher JK, Stephanopoulos G. Elementary metabolite units (EMU): a novel framework for modeling isotopic distributions. *Metab Eng*. 2007;9:68-86.
44. Young JD, Walther JL, Antoniewicz MR, Yoo H, Stephanopoulos G. An elementary metabolite unit (EMU) based method of isotopically nonstationary flux analysis. *Biotechnol Bioeng*. 2008;99:686-699.
45. Leighty RW, Antoniewicz MR. Parallel labeling experiments with U-^{13}C glucose validate *E. coli* metabolic network model for ^{13}C metabolic flux analysis. *Metab Eng*. 2012;14:533-541.
46. Leighty RW, Antoniewicz MR. COMPLETE-MFA: complementary parallel labeling experiments technique for metabolic flux analysis. *Metab Eng*. 2013;20:49-55.
47. Templeton N, Dean J, Reddy P, Young JD. Peak antibody production is associated with increased oxidative metabolism in an industrially relevant fed-batch CHO cell culture. *Biotechnol Bioeng*. 2013;110: 2013-2024.
48. Livak KJ, Schmittgen TD. Analysis of relative gene expression data using real-time quantitative PCR and the 2− ΔΔCT method. *Methods*. 2001;25:402-408.
49. Antoniewicz MR, Kelleher JK, Stephanopoulos G. Determination of confidence intervals of metabolic fluxes estimated from stable isotope measurements. *Metab Eng*. 2006;8:324-337.
50. Antoniewicz MR, Kelleher JK, Stephanopoulos G. Accurate assessment of amino acid mass isotopomer distributions for metabolic flux analysis. *Anal Chem*. 2007;79:7554-7559.
51. Zhang H, Badur MG, Divakaruni AS, et al. Distinct metabolic states can support self-renewal and lipogenesis in human pluripotent stem cells under different culture conditions. *Cell Rep*. 2016; 16:1536-1547.
52. Chaudhry MA, Bowen BD, Piret JM. Culture pH and osmolality influence proliferation and embryoid body yields of murine embryonic stem cells. *Biochem Eng J*. 2009;45:126-135.
53. Gupta P, Hourigan K, Jadhav S, Bellare J, Verma P. Effect of lactate and pH on mouse pluripotent stem cells: importance of media analysis. *Biochem Eng J*. 2017;118:25-33.
54. Huckabee WE. Control of concentration gradients of pyruvate and lactate across cell membranes in blood. *J Appl Physiol*. 1956;9: 163-170.
55. Halestrap AP. The monocarboxylate transporter family—structure and functional characterization. *IUBMB Life*. 2012;64:1-9.
56. Draoui N, Feron O. Lactate shuttles at a glance: from physiological paradigms to anti-cancer treatments. *Dis Model Mech*. 2011;4: 727-732.
57. Turner J, Quek LE, Titmarsh D, et al. Metabolic profiling and flux analysis of MEL-2 human embryonic stem cells during exponential growth at physiological and atmospheric oxygen concentrations. *PLoS One*. 2014;9:13.
58. Gaspar JA, Doss MX, Hengstler JG, Cadenas C, Hescheler J, Sachinidis A. Unique metabolic features of stem cells, cardiomyocytes, and their progenitors. *Circ Res*. 2014;114:1346-1360.
59. Glacken M, Adema E, Sinskey A. Mathematical descriptions of hybridoma culture kinetics: I. initial metabolic rates. *Biotechnol Bioeng*. 1988; 32:491-506.
60. Hassell T, Gleave S, Butler M. Biotechnology, growth inhibition in animal cell culture. The effect of lactate and ammonia. *Appl Biochem Biotechnol*. 1991;30:29-41.
61. Metallo CM, Walther JL, Stephanopoulos G. Evaluation of ^{13}C isotopic tracers for metabolic flux analysis in mammalian cells. *J Biotechnol*. 2009;144:167-174.
62. Ivarsson M, Noh H, Morbidelli M, Soos M. Insights into pH-induced metabolic switch by flux balance analysis. *Biotechnol Prog*. 2015;31: 347-357.
63. Mulukutla BC, Gramer M, Hu WS. On metabolic shift to lactate consumption in fed-batch culture of mammalian cells. *Metab Eng*. 2012; 14:138-149.
64. Mulukutla BC, Yongky A, Grimm S, Daoutidis P, Hu WS. Multiplicity of steady states in glycolysis and shift of metabolic state in cultured mammalian cells. *Plos One*. 2015;10:20.
65. Leite TC, Da Silva D, Coelho RG, Zancan P, Sola-Penna M. Lactate favours the dissociation of skeletal muscle 6-phosphofructo-1-kinase tetramers down-regulating the enzyme and muscle glycolysis. *Biochem J*. 2007;408:123-130.
66. Fendt SM, Bell EL, Keibler MA, et al. Reductive glutamine metabolism is a function of the α-ketoglutarate to citrate ratio in cells. *Nat Commun*. 2013;4:11.
67. Mintun MA, Vlassenko AG, Rundle MM, Raichle ME. Increased lactate/pyruvate ratio augments blood flow in physiologically activated human brain. *Proc Natl Acad Sci*. 2004;101:659-664.
68. Wise DR, Ward PS, Shay JES, et al. Hypoxia promotes isocitrate dehydrogenase-dependent carboxylation of α-ketoglutarate to citrate to support cell growth and viability. *Proc Natl Acad Sci U S A*. 2011; 108:19611-19616.
69. Fan J, Kamphorst JJ, Rabinowitz JD, Shlomi T. Fatty acid labeling from glutamine in hypoxia can be explained by isotope exchange without net reductive Isocitrate dehydrogenase (IDH) flux. *J Biol Chem*. 2013; 288:31363-31369.
70. Grassian AR, Parker SJ, Davidson SM, et al. IDH1 mutations Alter citric acid cycle metabolism and increase dependence on oxidative mitochondrial metabolism. *Cancer Res*. 2014;74:3317-3331.
71. Tohyama S, Fujita J, Hishiki T, et al. Glutamine oxidation is indispensable for survival of human pluripotent stem cells. *Cell Metab*. 2016; 23:663-674.
72. Pavlides S, Whitaker-Menezes D, Castello-Cros R, et al. The reverse Warburg effect aerobic glycolysis in cancer associated fibroblasts and the tumor stroma. *Cell Cycle*. 2009;8:3984-4001.
73. Chen Y-J, Mahieu NG, Huang X, et al. Lactate metabolism is associated with mammalian mitochondria. *Nat Chem Biol*. 2016;12: 937-943.
74. Faubert B, Li KY, Cai L, et al. Lactate metabolism in human lung tumors. *Cell*. 2017;171:358-371. e9.
75. Boyer LA, Lee TI, Cole MF, et al. Core transcriptional regulatory circuitry in human embryonic stem cells. *Cell*. 2005;122: 947-956.
76. Chambers I, Colby D, Robertson M, et al. Functional expression cloning of Nanog, a pluripotency sustaining factor in embryonic stem cells. *Cell*. 2003;113:643-655.
77. Niwa H, Miyazaki J, Smith AG. Quantitative expression of Oct-3/4 defines differentiation, dedifferentiation or self-renewal of ES cells. *Nat Genet*. 2000;24:372-376.
78. Chew J-L, Loh Y-H, Zhang W, et al. Reciprocal transcriptional regulation of Pou5f1 and Sox2 via the Oct4/Sox2 complex in embryonic stem cells. *Mol Cell Biol*. 2005;25:6031-6046.
79. Adachi K, Suemori H, Yasuda S y, Nakatsuji N, Kawase E. Role of SOX2 in maintaining pluripotency of human embryonic stem cells. *Genes Cells*. 2010;15:455-470.
80. Wang Z, Oron E, Nelson B, Razis S, Ivanova N. Distinct lineage specification roles for NANOG, OCT4, and SOX2 in human embryonic stem cells. *Cell Stem Cell*. 2012;10:440-454.
81. Kim H, Jang H, Kim TW, et al. Core pluripotency factors directly regulate metabolism in embryonic stem cell to maintain pluripotency. *Stem Cells*. 2015;33:2699-2711.

82. Hui S, Ghergurovich JM, Morscher RJ, et al. Glucose feeds the TCA cycle via circulating lactate. *Nature*. 2017;551:115-118.
83. Ahn WS, Antoniewicz MR. Metabolic flux analysis of CHO cells at growth and non-growth phases using isotopic tracers and mass spectrometry. *Metab Eng*. 2011;13:598-609.
84. DeBerardinis RJ, Mancuso A, Daikhin E, et al. Beyond aerobic glycolysis: transformed cells can engage in glutamine metabolism that exceeds the requirement for protein and nucleotide synthesis. *Proc Natl Acad Sci U S A*. 2007;104:19345-19350.
85. Mulukutla BC, Khan S, Lange A, Hu W-S. Glucose metabolism in mammalian cell culture: new insights for tweaking vintage pathways. *Trends Biotechnol*. 2010;28:476-484.

SUPPORTING INFORMATION

Additional supporting information may be found online in the Supporting Information section at the end of this article.

How to cite this article: Odenwelder DC, Lu X, Harcum SW. Induced pluripotent stem cells can utilize lactate as a metabolic substrate to support proliferation. *Biotechnol Progress*. 2021;37:e3090. https://doi.org/10.1002/btpr.3090